# "Computational Study of Surface Mechanical Attrition Treatment (SMAT) for AISI 304L Steel"

**M.Tech. Thesis**

By


**VIKESH KUMAR**

M. TECH (2017-2019)


**DISCIPLINE OF METALLURGY ENGINEERING & MATERIAL SCIENCE**

## INDIAN INSTITUTE OF TECHNOLOGY INDORE

**July-2019**

# "Computational Study of Surface Mechanical Attrition Treatment (SMAT) for AISI 304L Steel"

**A THESIS**

*Submitted in partial fulfillment of the requirements for the award of the degree*
***of***
**Master of Technology**

*By*

**VIKESH KUMAR**



**DISCIPLINE METALLURGY ENGINEERING & MATERIAL SCIENCE**

**INDIAN INSTITUTE OF TECHNOLOGY INDORE**


**July-2019**

# INDIAN INSTITUTE OF TECHNOLOGY INDORE

## CANDIDATE'S DECLARATION

I hereby certify that the work which is being presented in the thesis entitled **"COMPUTATIONAL STUDY OF SURFACE MECHANICAL ATTRITION TREATMENT (SMAT) FOR AISI 304L STEEL"** in the partial fulfillment of the requirements for the award of the degree of **MASTER OF TECHNOLOGY** and submitted in the **DISCIPLINE OF METALLURGY ENGINEERING & MATERIAL SCIENCE, Indian Institute of Technology Indore**, is an authentic record of my own work carried out during the time period from July 2017 to July 2019 under the supervision **Dr. Santosh S. Hosmani,** Associate Professor, IIT Indore and **Dr. Indrasen Singh**, Assistant professor, IIT Indore

The matter presented in this thesis has not been submitted by me for the award of any other degree of this or any other institute.

**Signature of the student with date**
**(VIKESH KUMAR)**

---

This is to certify that the above statement made by the candidate is correct to the best of my/our knowledge.

Signature of the Supervisor, with date　　　Signature of the Supervisor, with date

**(Dr. Santosh S. Hosmani)**　　　**(Dr. Indrasen Singh)**

---

**Vikesh Kumar** has successfully given his M.Tech. Oral Examination held **26 June 2019**.

Signature of Supervisor of M.Tech. Thesis　　　Convener, DPGC
Date:　　　Date:

Signature of PSPC Member 1　　　Signature of PSPC member 2
Date:　　　Date:

---

# ACKNOWLEDGEMENTS

I express my deep sense of gratitude to the Almighty for guiding me and giving patience throughout this duration. Inspiration and guidance are valuable in all aspects of life. This venture has received the hearty support of my Supervisors **Dr. Santosh S. Hosmani** and **Dr. Indrasen Singh.** Constant encouragement, motivation, and enthusiasm from my guide helped me to move forward with an investigation in depth. I take this opportunity to express my profound gratitude to **Prof. Pradeep Mathur**, Director, IIT Indore for providing the essential facilities, valuable guidance and cooperation.

I am extremely happy to express my gratitude towards my PSPC members **Dr. Shailesh I. Kundalwal** and **Dr. Hemant Borkar** for their guidance and support. I am thankful **Dr. Parasharam M. Shirage**, HOD, and Dept. of MEMS for his support and cooperation. I am thankful to all the faculty members of the Department of Metallurgy and Material Science for their guidance and support.

I acknowledge and thankful to **CAD LAB** for allowing me to conduct my simulation work and study. I am thankful to **MHRD, Govt of India** for providing fellowship during my Master studies.

Last but not the least, I cannot forget the support and encouragement received from my Family and my colleague **Mr. Digvijay Singh, Mr. Aditya Litoria, Mr. Manoj D. Joshi, S. Hirmukhe** (research scholars, IIT Indore) and **Mr. Mayur Dhake** without which this journey would not have been possible.

# Abstract

Surface mechanical attrition treatment (SMAT) is a surface treatment process widely used to enhance the mechanical properties of the material. In this study, Three-dimensional finite element model of single and multiple shot impacts are developed to investigate the effect of the SMAT process parameter. The single impact deformation model is used to investigate the relationship between impact deformation and the parameters involved in the SMAT processing, specifically shot size and impact velocity. To see the effect of multiple impacts of shot on the same position, single point multiple impact finite element model was developed. Since shot impact in SMAT has intrinsic random characteristics, a random sequence of shots must be taken into account for numerical modeling of multiple impacts. ABAQUS scripting using Python programming language was utilized to build a multiple impact model.

# TABLE OF CONTENTS

## Chapter 3 Scope Of The Study



## Chapter 4 Finite Element Modeling and Simulation



## Chapter 5 Result and Discussion

# LIST OF FIGURES

# LIST OF TABLES

# NOMENCLATURE

## List of Abbreviations and Symbols

| | |
|---|---|
| SP | Shot Peening |
| SMAT | Surface Mechanical Attrition Treatment |
| SPD | Severe Plastic Deformation |
| DDW | Dence Dislocation Wall |
| DT | Dislocation Tangles |
| UTS | Ultimate Tensile Strength |
| TWIP | Twinning Induced Plasticity |
| SFE | Stacking Fault Energy |
| $Y_s$ | Yield Strength |
| $\nu$ | Poisson Ratio |
| E | Youngs' Modulus |
| $\rho_t$ | Density |
| $\sigma$ | Dynamic Stress |
| $\sigma_o$ | Static Stress |
| $\dot{e}$ | Strain Rate |
| $\mu$ | Coefficient Of Friction |
| $\Delta t$ | Minimum Stable Time Increment |
| $L_{min}$ | Smallest Mesh Size |
| ALE | Arbitrary Lagrangian-Eulerian |
| PEEQ | Equivalent Plastic Strain |
| EQRS | Equivalent Residual Stresses |

| | |
|---|---|
| CRS | Compressive Residual Stress |
| KE | Kinetic Energy |
| PE | Potential Energy |
| $\theta$ | Incident Angle |

# CHAPTER I

# INTRODUCTION

## 1.1 Introduction

Stainless steels are important material because of their broad industrial applications. In industries, most of the engineering components deteriorate due to wear, fatigue or corrosion. To increase the service life of the engineering components, improvement of the surface properties of the material is required without affecting the bulk properties of the components. To achieve the above target surface engineering is very useful. Surface engineering is a technique which is useful to enhance the surface properties of the materials. Surface engineering can be defined as "*treatment of the surface and near-surface regions of a material to allow the surface to perform functions that are distinct from those demanded from the bulk of the material*" [1]. There are mainly three types of surface engineering techniques (i) surface coating (ii) surface modification, and (iii) surface hardening. Surface coating involves the addition of the desired material on the surface to accomplish prolonged surface properties, surface modification is a technique to bring an alteration to the material's surface properties without changing the chemistry of the material and surface hardening is the process of hardening of the surface with the help of flame, induction, electron-beam, and laser.

Surface modification technique such as rolling, shot peening (SP), hammering, surface mechanical attrition treatment (SMAT), etc. as shown in fig. 1.1, are used to enhance the surface properties of the material such as hardness, strength (without affecting the ductility of the material), fatigue properties, tribological properties (wear), etc. SMAT is similar to the shot peening process but there are some fundamental differences between SAMT and shot peening for example size of the shot, shot velocity, and direction of shot impact. Compare to other surface modification technique SMAT is a unique and low-cost process to increase the surface properties of the material because the input energy required to accelerate the shot is very less. For example in shot peening process velocity of the shot is 20-150 m/s but in the SMAT process velocity of the shot varies from 1 m/s to 20 m/s.

Surface Mechanical Attrition Treatment (SMAT) is a method of surface treatment which was introduced by K. Lu and Jian Lu around 1999 [2]. SMAT is a technique for producing nanostructure on the surface of the different metals and alloys such as iron and stainless steel [3, 4], copper [5] aluminum alloy [6]. SMAT is one of the surface treatment technique in which spherical shots are impacted randomly and multidirectional on the surface of the material with the help of vibration generator as shown in fig.1.2 [7]. During the SMAT randomly moving shot create very high strain rate $10^3$ to $10^5$ $s^{-1}$ on the material [8] and due to this high strain rate, dislocation or deformation induced twins are generated on top of the SMATed surface. These mechanically induced twins and dislocation form nano-structured near the top of the treated surface. Due to this nano-structured layer and compressive residual stress many mechanical properties significantly increases such as fatigue [9], wear [10], and surface hardness [11].

Finite element simulation is used, to understand the most influencing process parameter involved in SAMT and also see the effect of the SMAT parameter in the treated material such as residual stress, equivalent plastic strain, and deformation of the material. The computational modeling has been mainly used for many manufacturing processes including SMAT, in order to avoid the cost and time associated with the trial-and-error approach.

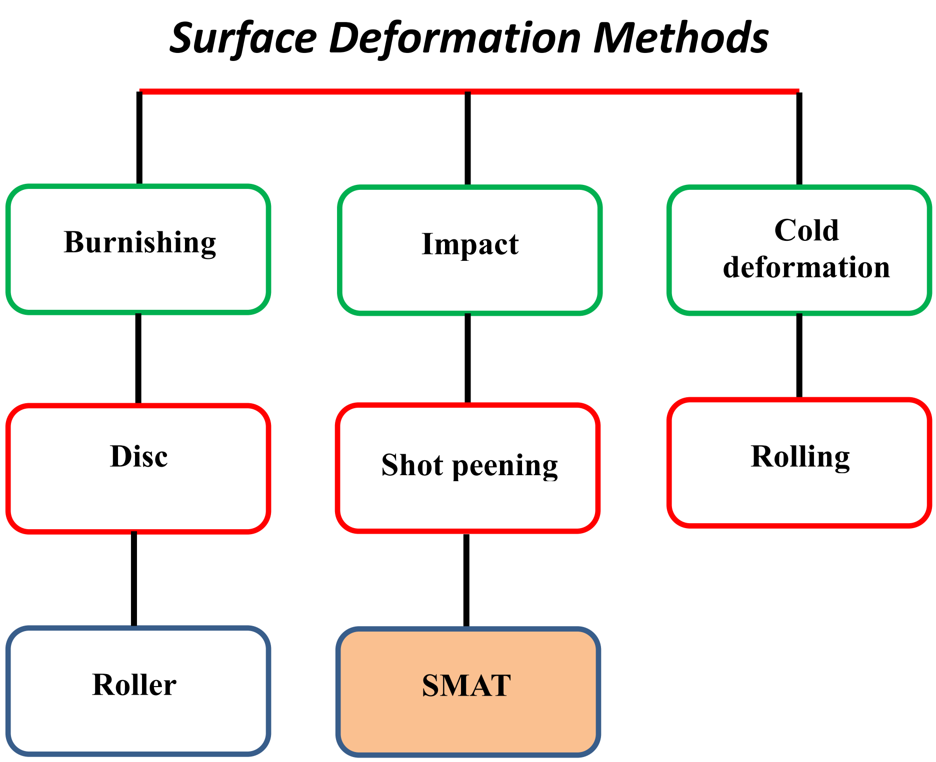


Figure 1.1: Mechanical Methods for Surface Modification.

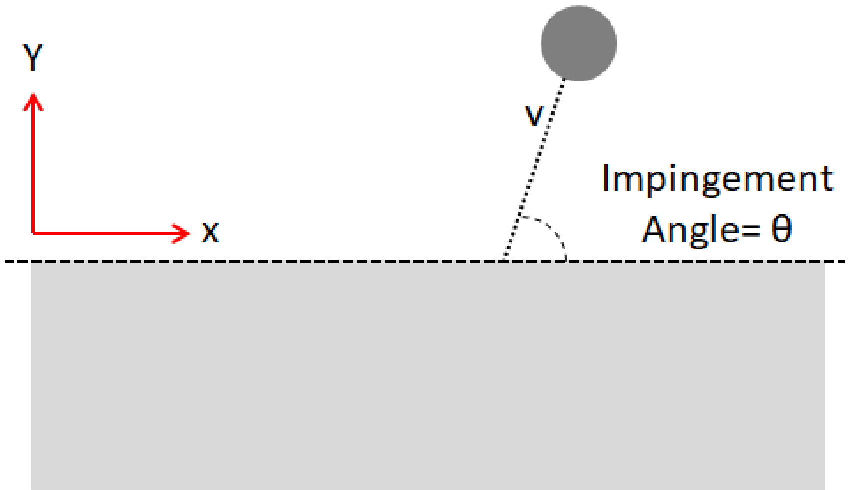


Figure 1.2: Single shot impacting on the target with a certain velocity at specified angle [12].

# Chapter 2

# LITERATURE REVIEW

This literature review is about surface engineering techniques. The main focus of this literature review is a mechanical method of surface modification by experimentation and the finite element method.

## 2.1 Surface Engineering Techniques

Surface engineering involves a modification in the volume of material on the top of the surface by the different type of surface engineering process. Surface engineering methods may be classified in terms of those which result in [13] :

(i) Modification in the constitution of a surface layer.
(ii) Constitutional, as well as Chemical a modification in a surface layer.
(iii) Different material deposited on to the original surface.
(iv) Compressive residual stresses (CRS).

There are generally two types of approaches in surface engineering techniques, which is a top-down approach and a bottom-up approach. Surface modification technique is the top-down approach of surface engineering technique. Surface engineering technique is divided into 6 groups (fig.2.1), which depend on the utilization of layer in surface engineering

| Surface Engineering Methods | | | | | |
|---|---|---|---|---|---|
| ***Mechanical*** | ***Thermo-mechanical*** | ***Thermal*** | ***Thermo-chemical*** | ***Electro-chemical and chemical*** | ***Physical*** |
| Burnishing<br>- Disk burnishing<br>- Roller Burnishing<br><br>Impact<br>- Shot peening<br>- Surface mechanical attrition treatment(SMAT)<br>- Hammering<br><br>Detonation<br><br>Cold deformation<br>-Rolling<br>-Forging | Thermal spraying<br>- Gas<br>- Arc<br>- Plasma<br><br>Spray melt coating (padding)<br><br>Plating<br>- Thrust rolling (Extrusion broaching)<br>- Detonation<br>- Shrinkage<br><br>Hardening<br>- Laser<br>- Electron beam<br>- Explosive<br><br>Hot reduction<br>- Rolling<br>- Forging | Hardening, Tempering, Annealing<br>- Induction<br>- Flame<br>- Plasma<br>- Laser beam<br>- Electron beam<br>- Resistance<br><br>Surface remelting (glazing)<br>- Laser beam<br>- Electron beam<br>- Flame<br>- Plasma<br><br>Pad welding<br><br>Melt coating<br>- Laser beam<br>- Electron beam<br>- Spark discharge<br><br>Melting<br><br>Hot dip coating (hot dip metallizing) | Saturation<br>- By diffusion unassisted<br>Powder<br>Salt bath<br>Gas<br>- By diffusion assisted<br>Glow discharge<br>CVD techniques<br><br>Melt alloying<br>- Laser beam<br>- Electron beam<br>- Plasma<br><br>Thermo-chemical setting | Deposition<br>- Electrolytical<br>- Chemical<br>- Conversion<br><br>Polishing<br>- Chemical<br>- Electrochemical<br><br>Etching<br>- Chemical<br>- Electrochemical<br><br>Chemical setting<br><br>Sol-gel techniques | Physical setting<br><br>Vapor deposition<br>- Evaporation<br>- Ion plating<br><br>Implantation of ions(ion alloying)<br>- Simple ion implantation<br>- Recoil ion implantation<br>- Ion mixing |

Figure 2.1: Classification of surface engineering method by method of layer generation [14].

## 2.2 Mechanical Methods for Surface Modification

Mechanical method for surface modification technique in which very fine grain structure is generated near the top of the surface of the material by applying some mechanical forces on the top surface of the material. Due to mechanical force, large plastic strain is introduced on the surface of the material and this plastic strain helps to develop the refinement of the grain in the material near the surface. By this method surface hardness and overall strength of the material is improves without much change in ductility [15, 16]. There is some mechanical method for surface modification are rolling, shot peening, SMAT, etc.

### 2.2.1 Rolling

Rolling is a severe plastic deformation process in which spherical or cylindrical roller is used to deform the surface of the material by applying some mechanical pressure on the roller (fig. 2.2). This process improves surface properties of the material for example hardness, strength, and fatigue resistance by induced residual compressive stress and work hardening.

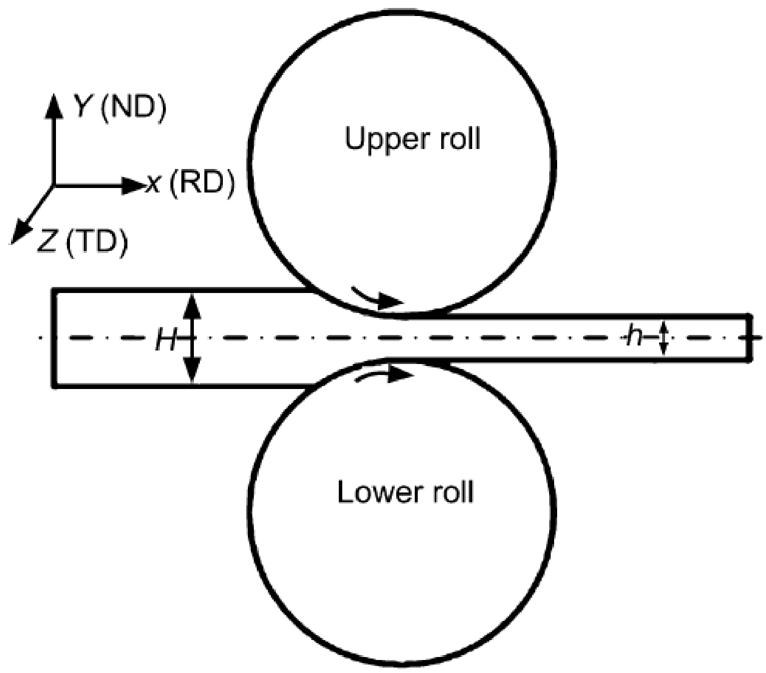


Figure 2.2: Schematic diagram for the cold rolling process.

Rolling process is an expensive process to enhance the mechanical properties of the material. Due to boosted compressive residual stress (CRS) in the material, improvement of fatigue property has been observed [17], but this process has some limitation like for irregular shape of the material.

### 2.2.2 Shot Peening (SP)

Shot peening (SP) is a cold working process which involves the impact of metallic, glass, or ceramic shot, which may be spherical, cylindrical, or irregular shape on the surface of the material (fig.2.3). This process commonly used for surface treatment of the material in aerospace industries to increase the fatigue properties of the engineering components because of delay of crack initiation and crack propagation rate [18]. In the shot peening (SP) method the size of the shot is very small (0.1-1 mm) and the shape of the shot is not necessary to be spherical. In this technique, compressive residual stress (CRS) is developed on the surface to increase the fatigue properties of the material (fig.2.4).

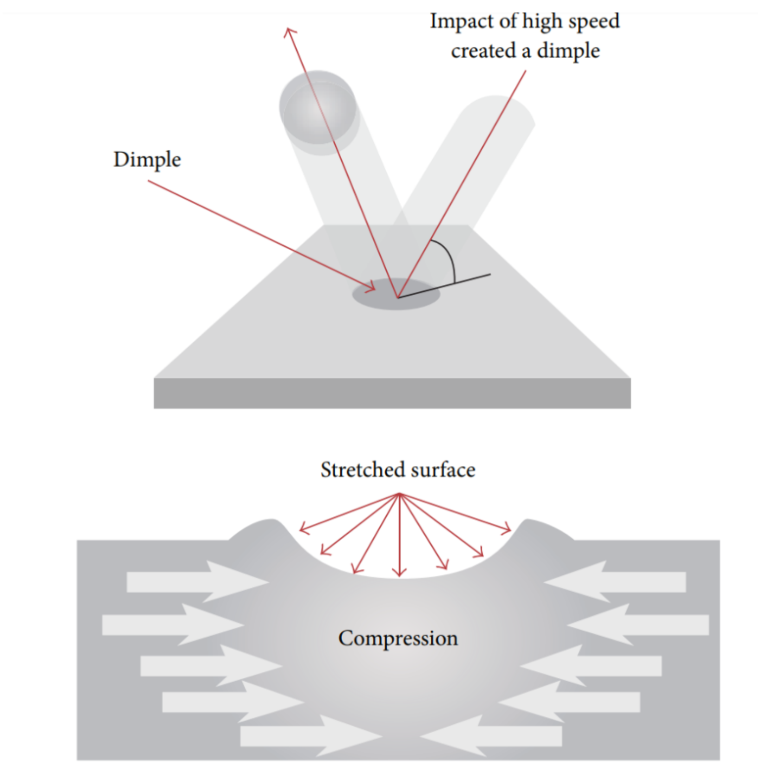


Figure 2.3: Schematic diagram of shot peening, spherical shot impact on a surface with some velocity [18].

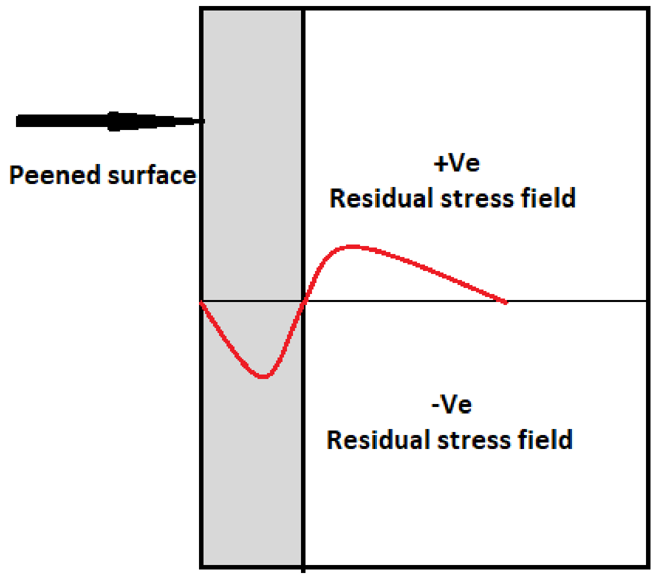


Figure 2.4: Schematic of residual stress distribution below a peened surface [19]

### 2.2.3 Surface Mechanical Attrition Treatment (SMAT)

SMAT is one of the surface modification techniques which are used to enhance the surface properties of the material due to the help of severe plastic deformation (SPD) by using the impact of randomly moving shots and by this severe plastic deformation (SPD) the grain refinement occurs near the top of the surface. Nano-level of grain refinement has been observed by the SMAT process. In the SMAT (fig.2.5) the size of the ball is much larger (1-8 mm) than ball size involved in shot peening. In this technique, a large amount of dislocation or deformation induced twin is generated near the surface. During the SMAT process, nono size grain structure is observed on the top of the surface and rest of the material microstructure is unchanged. Due to this gradient in the microstructure, the surface provides the desirable properties on the surface depth up to ~ 10-50 µm.

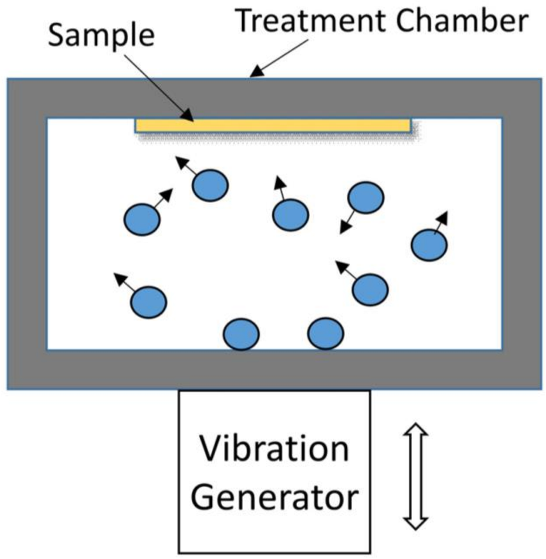


Figure 2.5: Schematic diagram of the SMAT working principle.

In the SMAT ball/shot are vibrated in the SAMT chamber with the help of vibration generator. Vibration generator generates vibration and transfers its energy to the ball after getting energy from the vibration generator ball impact from the random direction with a certain velocity on specimen which is held on top of the chamber.

## Comparison between SMAT and Shot Peening (SP)

The working principle of SP (shot peening) and SMAT is a similar process. However, it differs from each other in many aspects, which are as follows:

**Size of the shot/ball –** the size of the ball in SAMT is larger (1-8 mm) then the size of the ball in shot peening (0.1-1 mm). In the shot peening, the shape of the ball is not necessary to be spherical it may be in any shape but in SMAT shape of the shot is spherical.

**The velocity of the shot/ball** – in SMAT the ball velocity is in the range of 1.0–20.0 m/s however, in shot peening the velocity of the ball is around 150.0 m/s.

**Duration of the process –** in SMAT duration of the process varies from 10-180 min. however, in shot peening is done in few seconds to minutes.

**The direction of impact –** in shot peening the direction of impact of ball is near about perpendicular to the treated surface but in SMAT the impact of shot is multi-direction.

Table 1: Comparison between SMAT and shot peening with different parameter

| **Parameters** | **Shot Peening** | **SMAT** |
|---|---|---|
| **Shot size (mm)** | 0.1-1 | **3-10** |
| **Shot velocity (m/s)** | 20-150 | **1-20** |
| **Spherical Shot shape** | Not necessary | **Necessary** |
| **Impact direction** | 90° | **Multidirectional** |
| **Treatment time** | Few seconds | **5 – 180 min** |
| **Hardness improvement** | negligible | **considerable** |

## Surface Nano Crystallization during SMAT

during SMAT when ball impacts on the surface of the material the maximum strain rate and strain are induced on the surface, and along with the depth, the strain is decreasing because strain rate decreases from surface to depth of the material. Due to this microstructure gradient was found, it has mainly four layer of the SAMTed material which are as follows:

- Nano-grains at the top surface
- Refined structure.
- The deformed coarse grains.
- Strain-free coarse-grains matrix.

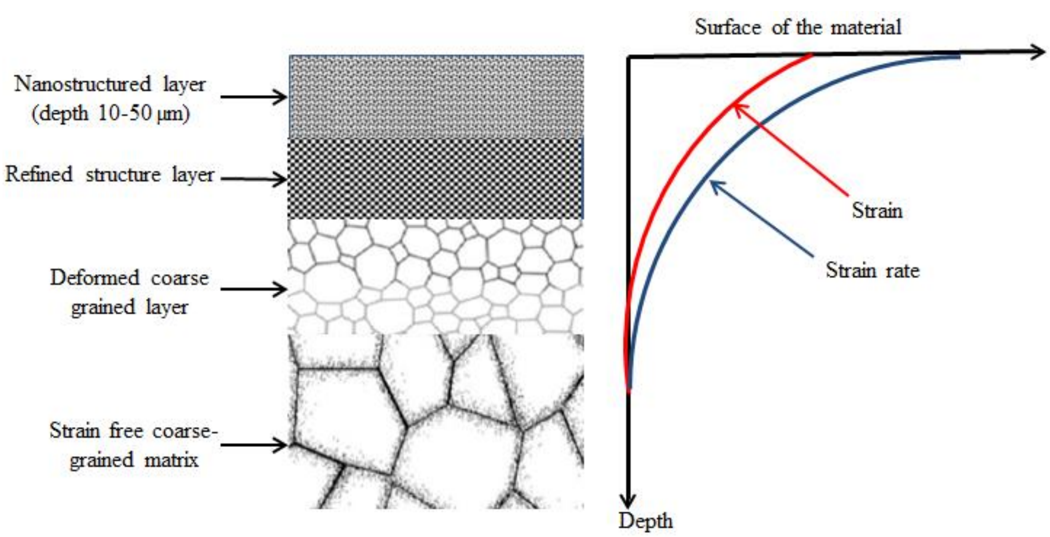


Figure 2.6: Schematic figure of microstructure gradient and distribution of strain rate and strains along with the thickness in the surface layer of the SMATed material. [20]

# SMAT Induced Nano-Grain Generation Mechanism

The grain refinement mechanism depends on the stacking fault energy (SFE) of the material [8]. There are two types of nano-grain generation mechanism, for low stacking fault energy material and high stacking fault energy material. For low stacking fault energy material grain refinement occurs due to deformation induced twinning whereas for high stacking fault energy material grain refinement occurs due to the accumulation of dance dislocation wall (DDW) and dislocation tangles (DT) [8]. For high SFE material (SFE~ 200 mJ/mm$^2$) grain refinement mechanism is shown in fig.2.7

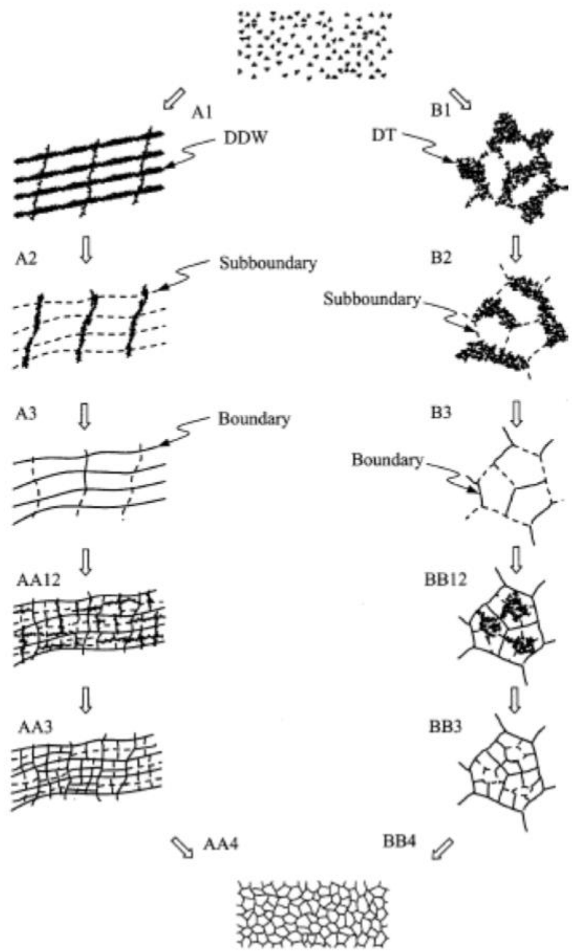


Figure 2.7: mechanism of Grain refinement in high SFE material [8].

For high SFE material like Fe, Al, etc. grain refinement occurs in the following steps:

1. Development of dislocation in the material
2. Accumulation of dislocation which forms dense dislocation wall or dislocation tangles within the grain
3. Transformation of dance dislocation wall or dislocation tangles into sub-grain boundaries in the grain.

By these following steps, the nano-grain structure is observed on the surface of the SMATed material. The grain refinement observed up to 10-50 µm from the treated surface [22].

For low SFE material like steel (AISI 304), copper, magnesium, etc. grain refinement is shown in fig 2.8. In low SFE material, the grain refinement occurs due to the development of twins within the grain. In low SFE material (SFE~ 17.0 $mJ/m^2$), mechanical induced twins are generated within the grain. This twin-twin interaction (rhombic block) which is shown in fig. 2.8 in stape 2 behaves as sub grain in the coarse grains. This boundary looks quite different from the dislocation boundary which can see in low SFE material [21]

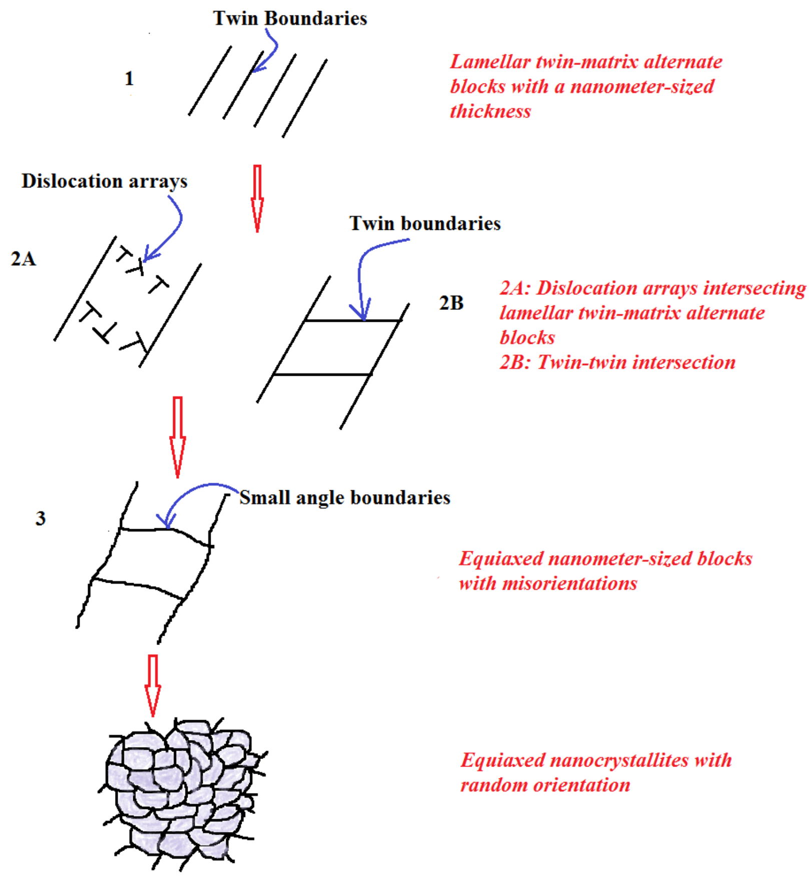


Figure 2.8: Grain refinement mechanism in low SFE material [8].

## 2.3 Experimental Study on SMAT

SMAT is a technique of surface treatment which was first introduced by Jian Lu and K. Lu in 1999. To understand improvement in properties of the SMATed specimen many researchers have done experimental work.

### 2.3.1 Microstructure of the SMATed Specimen

In figure 2.9 optical micrograph has been shown of the cross-section of the SMATed AISI 304L steel. This SMAT process has been done with 3 mm diameter of shot for 60 min SAMT time. As shown in figure 2.9, the shear band density near the treated surface is very much high as compare to the depth of the SMATed material. This shear/deformation band near the surface (0-0.3µm) of the treated material is mechanical induced twins.

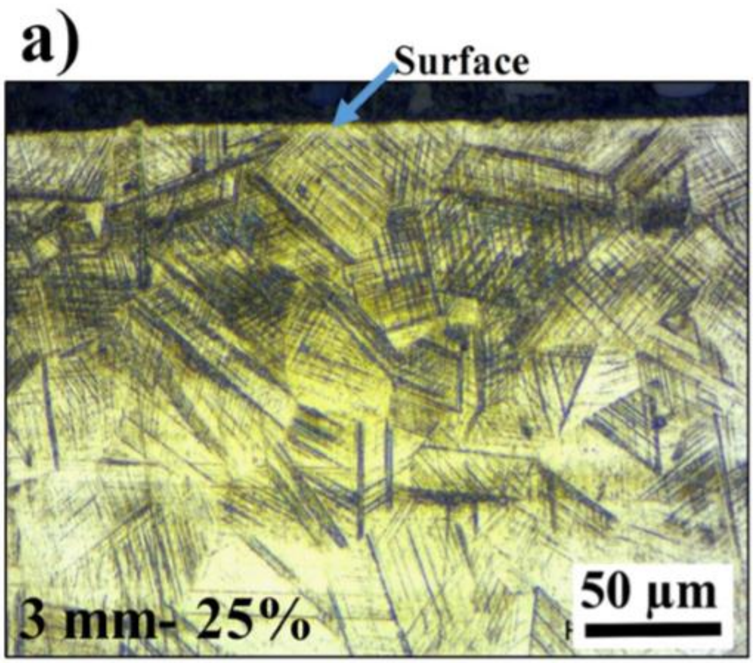


Figure 2.9: Optical micrograph of SMATed AISI 304L steel sample with 3mm shot diameter [23].

## 2.3.2Hardness of the SMATed Specimen

In this work, the SMAT process has been done on AISI 304L steel with 3 mm and 8 mm diameter shot for 60 min SMAT time and the velocity of the 8 mm shot was 50% lesser than the velocity of the 3 mm shot. In fig.2.10 shown the hardness profile of the SMATed material along with the depth. Near the surface of the treated material up to 100µm, the hardness of the material which is treated from 3 mn diameter shot is larger than the 8 mm diameter shot, which is because of the velocity of the shot for 3 mm shot is larger than 8 mm diameter shot, so the strain generated by 3 mm shot is more compare to the 8 mm shot. After the 100 µm, the hardness of the material which is treated from 8 mn diameter shot is larger than the 3 mm diameter shot, which is because of the higher energy of 8 mm shot, due to more mass of 8 mm shot as compared to the 3 mm shot. With the increase in hardness due to the SMAT, it influences the wear properties and friction properties [24, 25, and 26].

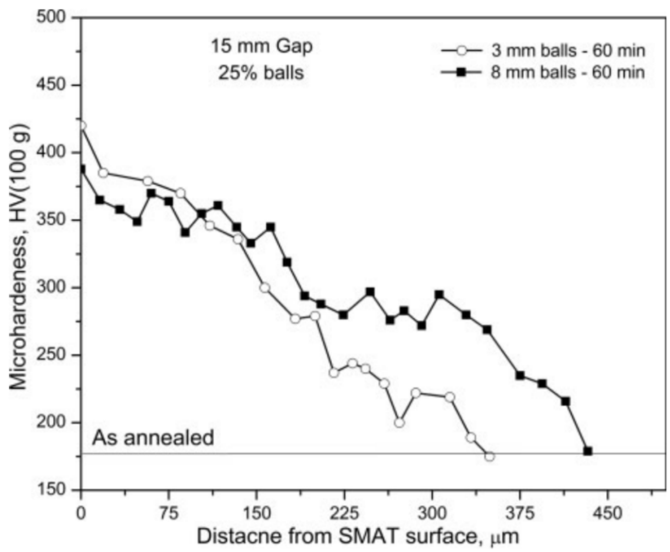


Figure 2.10: Microhardness along with the depth of cross-section of SMATed AISI 304L steel specimens using 3 and 8 mm diameter balls [23].

## 2.3.3 Strength of the SMATed Specimen

In this study [27], SMAT process was done with 5 mm shot diameter, which was used to enhance the yield strength of TWIP (twinning induced plasticity) steels. Fig. 2.11 shows that engineering stress-strain curve for SMATed, non-SMATed, and 10% cold rolled material. Due to this SMAT process, the yield strength of the material is increased from 400.0 ± 25.0 MPa to 550.0 ± 25.0 MPa and the ultimate tensile strength (UTS) is increased from 1040.0 MPa to 1140.0 MPa with a decrease of 8% total tensile deformation which is not much significant for the SAMT process. For 10 % of cold rolled material, the yield strength is very much similar to the SMATed material but the ductility is very poor in the case of cold rolled material. It is also reported that the increase in the yield strength for AISI 316 steel is 6 times due to the SMAT process [28]

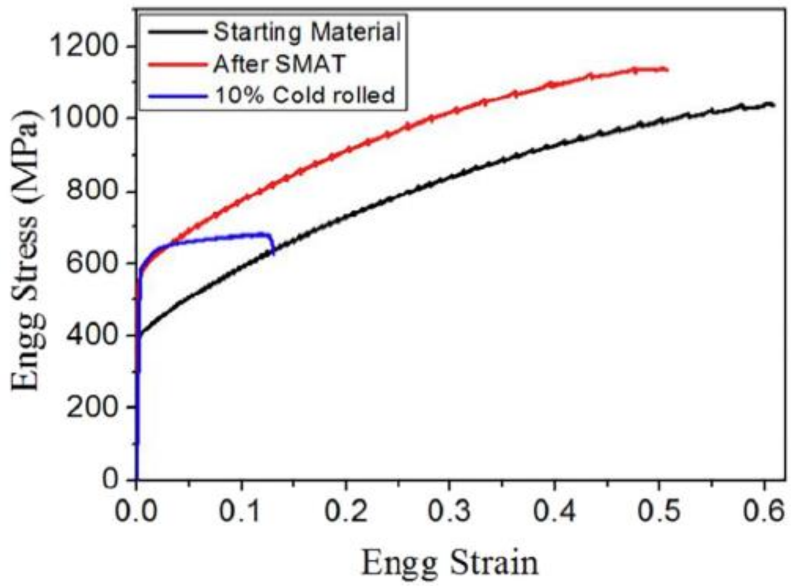


Figure 2.11: Comparison of engineering stress-strain curves for non-SMATed, SMATed and 10% cold rolled sample [27].

### 2.3.4 Fatigue Strength of SMATed Specimen

In this study [29], the fatigue behavior of 316L steel was studied on Nano-crystalline surface of the SMATed sample. Fig 2.12 shows that the S/N curve for the different treated condition under the limit of $N=2x10^6$ cycle. As shown in fig. 2.12 the fatigue limit of non-SMATed is 300 MPa and due to the SMAT process, 21% of improvement in fatigue limit has been observed when treated with 3 mm shot diameter [29]. During the SMAT with 3mm shot increase in fatigue limit for both low and high amplitude stress also improved the yield strength from 300MPa to 665MPa with good ductility has been observed. It is also observed that 13.1% of improvement of fatigue strength of carbon steel during the SMAT process [30]

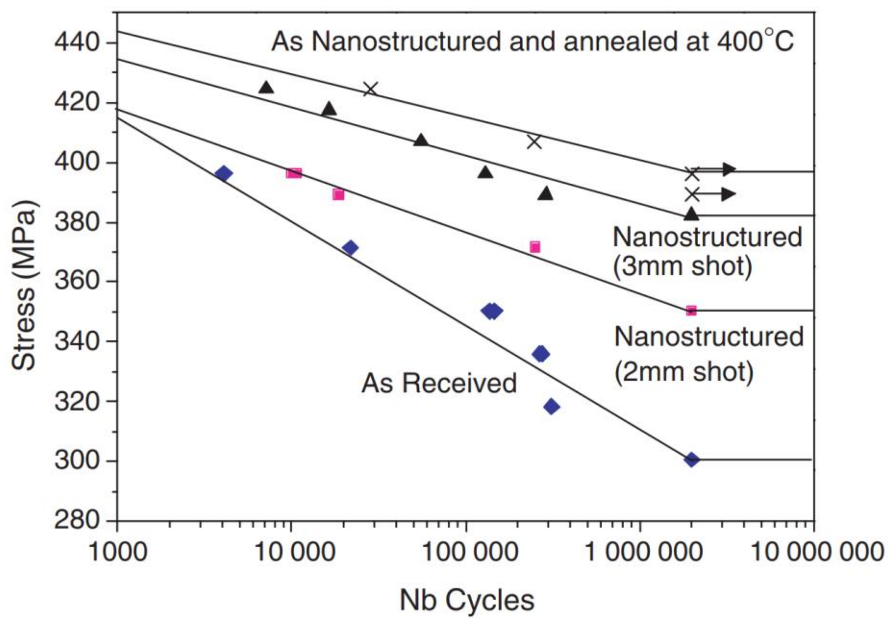


Figure 2.12: S/N curves of different SMATed samples and SMATed samples combined with annealing [29].

### 2.3.5 Wear Rate of SMAted Sample

In this paper [31], performances of the wear on the nano- crystallized surface specimen in dry sliding wear and wear in a 3.5 wt % NaCl solution was studied. Fig. 2.13 shows the wear rates ($mm^3/m$) of the SMAted sample along with the depth from the treated surface in air and in the NaCl solution. As shown, the wear rate near the treated surface was lower in both the cases, where the grain size was at the nanometer scale. The wear resistant depends on the hardness of the material and from previous literature have seen that the hardness profile along with the depth of the SMATed material.

Surface Nanocrystallization also decreased the coefficient of friction due to the decrease of the contact area with enhance in hardness and the decrease in the surface adhesive force when a more protecting passive film created on the nano-crystallized surface.

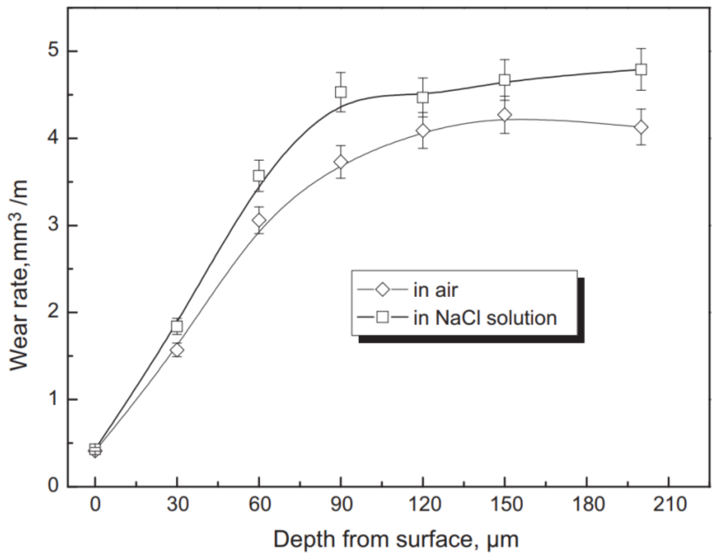


Figure 2.13: Wear rates of SMATed sample with the depth from the top surface measured in dry and in a NaCl solution. [31].

## 2.4 SAMT Modeling

SMAT is a dynamic work hardening surface treatment process. Initially, most of the researcher worked on the SMAT experimental method to see the effect of SMAT on different properties like hardness, fatigue strength, tribological properties (wear), the strength of the SMATed material, corrosion resistance, etc., but from past two-three year some of the researchers starts working on numerical simulation method to see the effect of SMAT parameter.

In this paper [32], single, as well as multiple shot impact models were performed using finite element code ABAQUS EXPLICIT 6.14 for aluminum AA1050-O material. In this study 2 mm of the analytical rigid shot is used with the velocity of 3.6 m/s at $90^0$ of impact angle. In fig. 2.14 (a) shows the residual stress distribution of the SMATed sample along with the depth just below the center of impact for different element size. In this profile near the treated surface, negative stress is developed and for higher depth, positive residual stress is developed to balance the stresses in the material [33]. In fig. 2.14(b) shows the variation in the surface displacement of the SMATed sample for different element size by the 2 mm diameter shot and 3.6m/s shot velocity. Fig. 2.14 (c) and (d) shows the distribution of equivalent plastic strain (PEEQ) along with the depth and along the surface of the SMATed material for the different element size. In this curve, PEEQ was initially increasing than after some point starts decreasing for both along with the depth and along the surface. From fig 2.14 has been observed that there is no change in the value of stress, displacement, and PEEQ with change in element size.

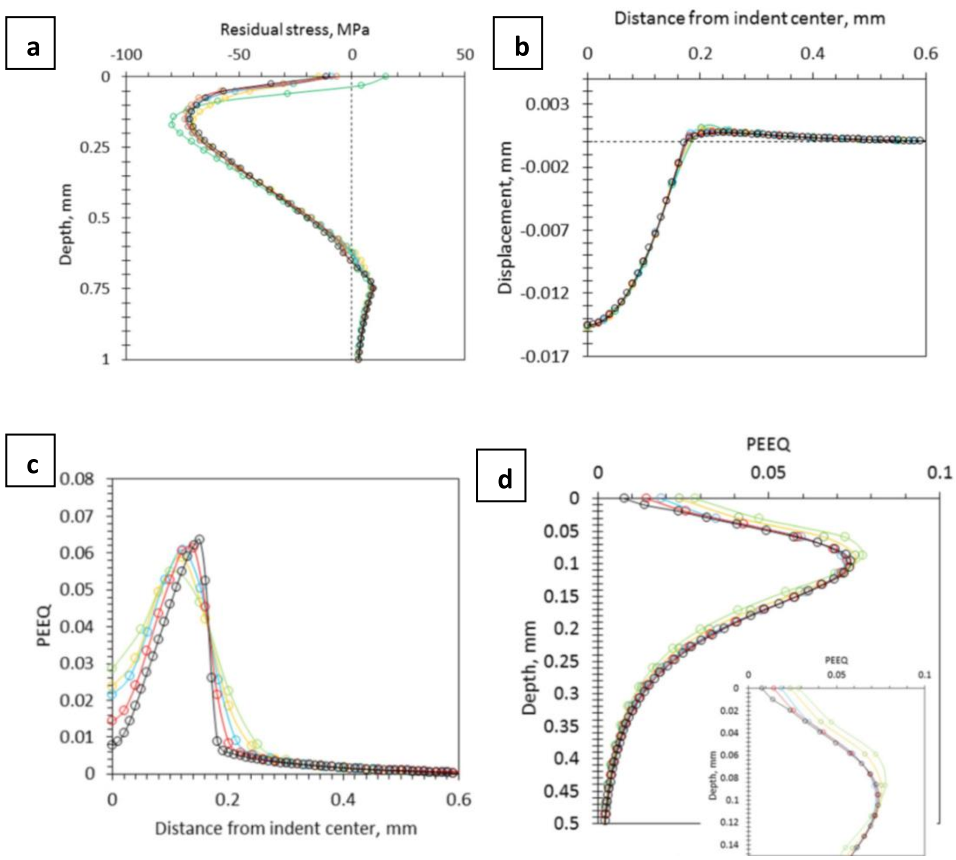


Figure 2.14: (a) Residual stress of the SMATed sample along with the depth, (b) surface displacement of the SMATed sample, the equivalent plastic strain of the SMATed sample (c) along with the surface, and (d) along with the depth with different element size [32].

Fig. 2.15 (a) shows the comparison between numerical and experimental residual stress along with the depth at 8 peening intensity. At the surface value of the residual stress is around -47 MP and maximum residual stress is -90 MP at 0.2 mm of depth from the top surface. Fig. 2.15 (b) shows the equivalent plastic strain along with the depth and surface for different peening intensity/coverage.

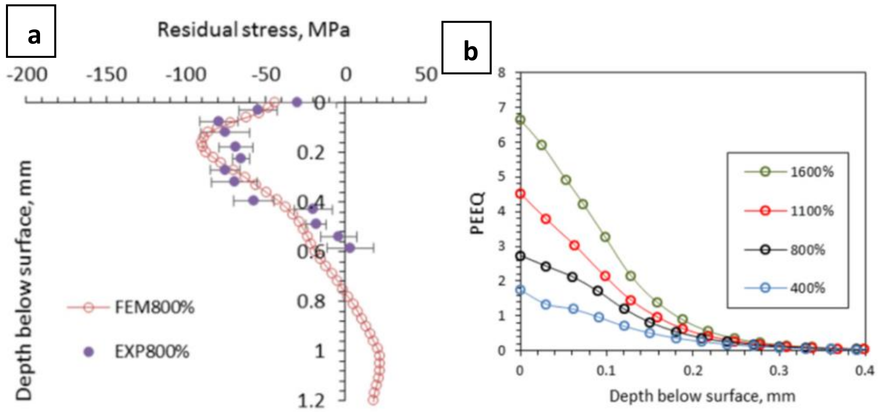


Figure 2.15: Shows, (a) the comparison of residual stress by the finite element method and experimental method along with the depth of the treated material for peening intensity of 8, (b) PEEQ distribution with the depth for different peening intensity/coverage.

In this study [34], the evolution of PEEQ (equivalent plastic strain) has been observed. For this three shot position were taken to see the effect. It can be seen that maximum PEEQ value is not observed at the center of impact, but it observed near the center of impact.

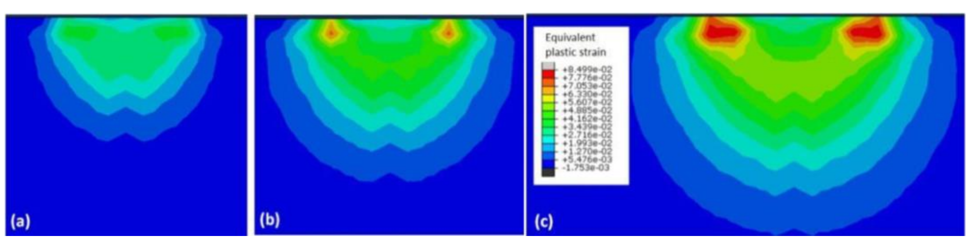


Figure 2.16: The equivalent plastic strain evolution, during the impact of the shot on the target [34].

In this study [35], comparison of Kirk and Iida empirical equation [36 and 37] with the indent diameter and indent depth, obtain from the single impact finite element analysis has been done. For the comparison study, 0.6 mm of shot diameter with varying shot velocity (6-9 x$10^4$ mm/s) at $90^0$ impact angle was used for 39NiCrMo3 steel. The Kirk and Iida formulae provide almost identical estimations for indent diameter but slightly diverge for the estimation of indent depth at higher velocities.

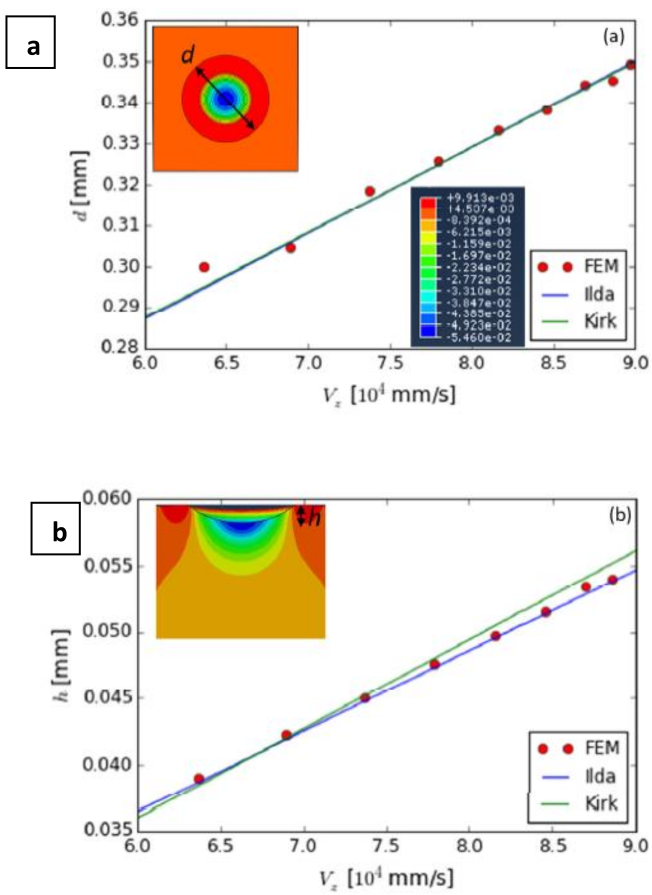


Figure 2.15: Comparison of the empirical equations of Kirk and Iida with the indent diameter and indent depth by with the data obtained from the single impact finite element model (FEM) analysis [35].

In this study [38], the effect of the constitutive material model used to describe the target material on the results obtained from the finite element numerical modeling of a shot peening process was analyzed. Different material model used to see the effect of indent diameter with variable shot velocity which is shown in fig. 2.16.

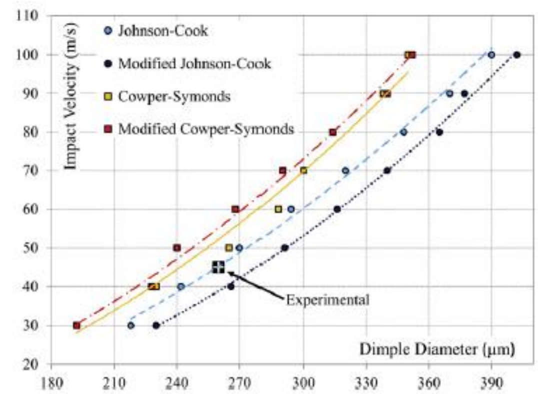


Figure 2.16: Indent diameter vs. shot velocity with different viscoplastic constitutive models.

# Chapter 3

## Scope of Study

In nowadays one of the major issues is developing innovative and cost-effective surface modification processes that can introduce better qualities to the surface of the material without altering its bulk properties.

In the SMAT process, optimization of process parameters needs to be done for low cost and time-saving methods for the surface modification. SAMT study is also carried out for different specimen material, also empirical relations can be drawn which can be useful for technological and industrial application.

During the literature review, it was found that most of the work has been done on the experimental part to see the effect of SMAT but very few studies have been done on the SMAT process by the computational technique.

### 3.1 Aim and Objectives of Study

Based on the gaps found during the literature survey, the aim of the present study is in-depth study of surface mechanical attrition treatment (SMAT) of AISI 304L steel. Considering the above aims, the following objectives are undertaken in the present study:

1. To model (single as well as multiple impact model) and simulate the surface mechanical attrition treatment (SMAT) process.
2. To study the effect of SMAT process parameters on the surface of the material and along with the depth of material.

## 3.2 Timeline for Study

Project Duration: **12 Months**

# July 2018 –June 2019

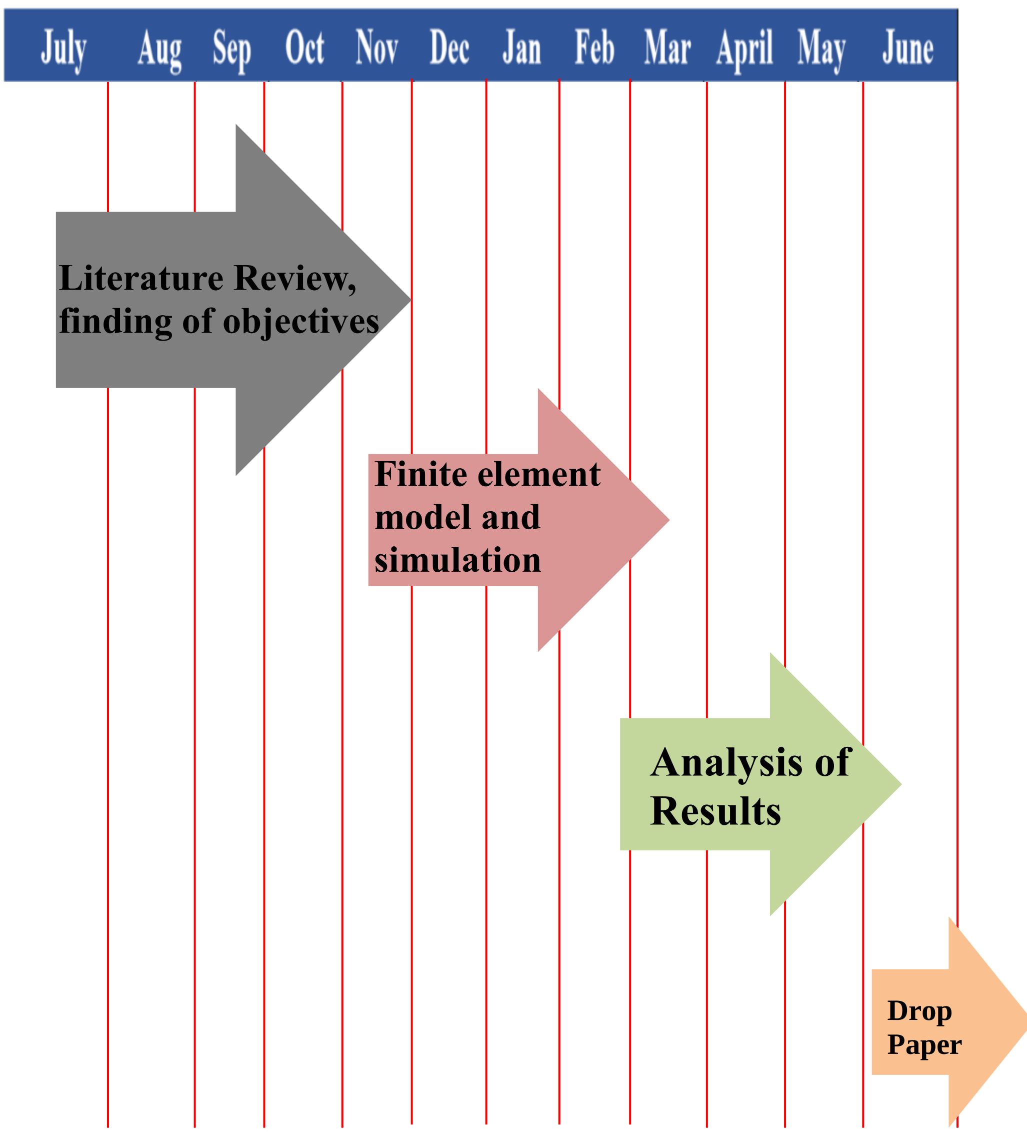

# CHAPTER 4

## FINITE ELEMENT MODELING AND SIMULATION

The modeling work described in this article had two parts. The first part consisted of a study of SMAT parameter with the help of Numerical model of SMAT and the second part is focused on evaluating the behavior of AISI 304 steel under the SMATed condition.

## 4.1 Numerical Model of Single Impact SMAT

For the development of the finite element model, the material property of AISI 304L steel were E = 200 GPa, ν = 0.26, and $\rho_t$ = 7850 kg/m$^3$ [39] and isotropic hardening was assumed where initial yield strength ($\sigma_0$) was set to 215 MPa and analysis were run with variable shot velocity (1, 5, 10, 15, m/s). Initial residual stresses and strain were assumed to be negligible.

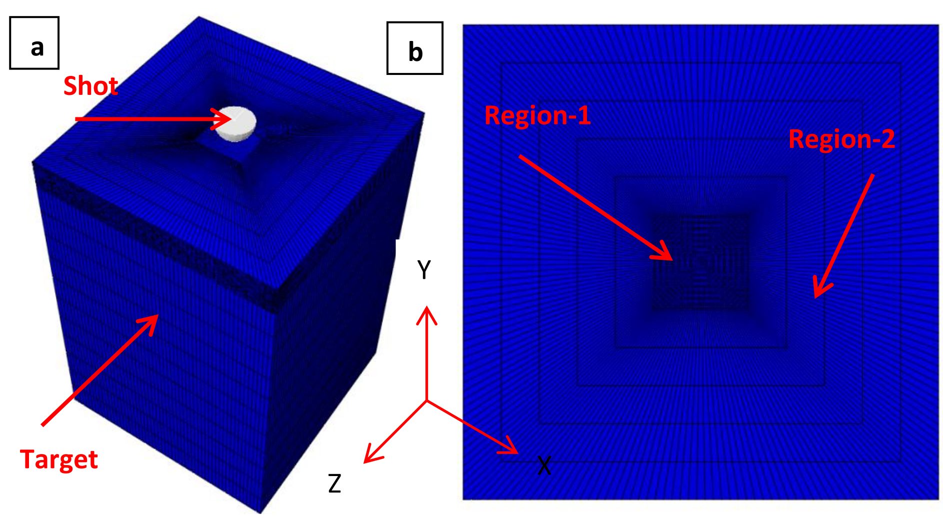


Figure 4.1: Finite element model showing (a) global view and (b) top view including target and rigid shot for single impact.

.

Three-Dimensional modeling and simulation were performed using finite element code ABAQUS Explicit 6.14 to investigate single as well as multiple impact process. This finite element model consisted of a square target face of 20 mm and height of 30mm as shown in fig. 4.1(a). To reduce the computational cost two regions were taken by the partition of the platform which is shown in fig. 4.1(b). Region-1 is an area where the ball is impacted on the surface of the material up to the depth of 1.5 mm. Here in region-1 mesh size is very fine as compared to the other region to reduce the number of the element.

## 4.2 Material Model and Material Properties

Material properties utilized to define the target material can be seen in table 4.1. The shot/ball (steel) was modeled as an analytical rigid body. It is important to notice that the strain rate can influence the mechanical properties of the material, during the SMAT strain rate is very high $10^3$-$10^5$ $S^{-1}$, determined by both experiments and numerical simulations [43, 44]. Therefore, modeling the target surface isotropic elastic-plastic material deformation model and Cowper-Symonds rate dependent material model was used for AISI 304L steel [32]. Jones (1989) presented that Cowper-Symonds parameter for AISI 304 steel as c =100 and p = 10 [40].

**Cowper–Symonds equation:** $$\boldsymbol{\sigma} = \boldsymbol{\sigma_0}\left[\mathbf{1} + \left(\frac{\dot{e}}{\boldsymbol{C}}\right)^{\frac{\mathbf{1}}{\boldsymbol{p}}}\right]$$

σ = Dynamic stress

$\sigma_o$ = Static stress

$\dot{e}$ = Strain rate

C and p are Cowper-Symonds coefficients

Table 4.1: Material parameters of the target AISI 304L steel for finite element modeling.

| **Target material** | |
|---|---|
| Material | AISI 304L steel |
| Young's Modulus (GPa) | 200 |
| Poisson's Ratio | 0.26 |
| Density (kg/m3) | 7850 |
| Thickness (mm) | 30mm |
| **Shot** | |
| Material | Steel (rigid) |
| Diameter (mm) (m) | Variable |
| Density (kg/m3) | 7850 |
| Velocity (m/s) | variable |

## 4.3 Contact Properties

The simulation of the SMAT was modeled using a dynamic explicit procedure. The contact of the shot/ball to the target material was managed through 'surface-to-surface' explicit contact, with 'tangential' behavior by penalty contact method with a coefficient of friction $\mu = 0.2$ [44]. Regarding frictional behavior, it is observed that differences in induced stresses were negligible for $0.1 \leq \mu \geq 0.5$ [41, 42]. In this finite element model, shot/ball was taken as the first surface and top of the target material was taken as the second surface, which is shown in fig. 4.2

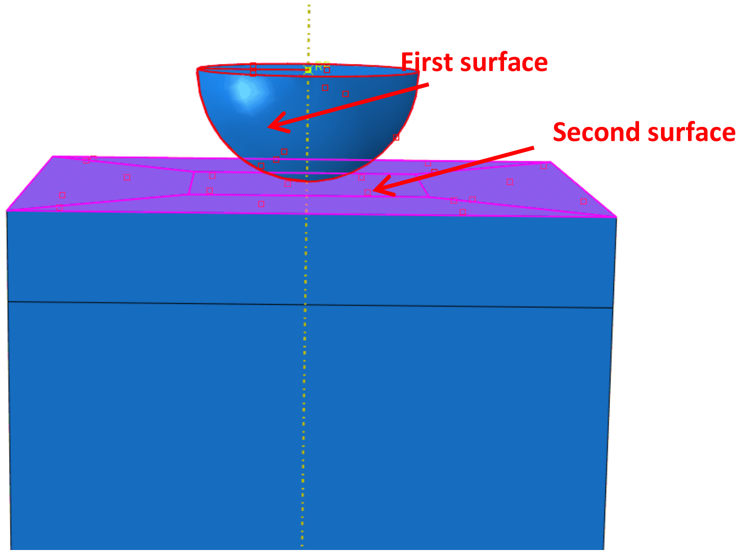


Figure 4.2: Shows the surface-to-surface contact between the shot and the target material.

## 4.4 Step in SMAT Modeling

In this finite element model, the basic time period t=0.02 were taken and for isotropic material, the minimum stable time increment Δt depends on the mesh size and material properties and can be evaluated as:

$$\Delta t = l_{min}\sqrt{\frac{\rho}{E}}$$

Where Δt is minimum stable time increment

$L_{min}$ is the smallest mesh size

ρ is the density of the material

E is Young’s Modulus of the target material

## 4.5 Mesh in SMAT Modeling

The partitions of the target were allowed for refining of the mesh near to the point of contact between target and shot. Figure 4.3 shows the mesh of the target material, near the contact of shot and target very fine mesh has been done and for the rest of the area coarse mesh has been done to reduce the number of elements in the model. Due to less number of elements, the overall computational cost is reduced.

Table 4.2: Mesh size and mesh type according to the region.

| Mesh type | Mesh size | Location, x-z |
|---|---|---|
| Fine | 0.07 | Region-1 |
| Coarse | 2.7 | Region-2 |

In this model, target meshed with 3-D explicit C3D8R (Eight-node reduced-integration brick element). Arbitrary Lagrangian-Eulerian (ALE) adaptive meshing technique was also incorporated to control element distortion due to large deformations during SMAT.

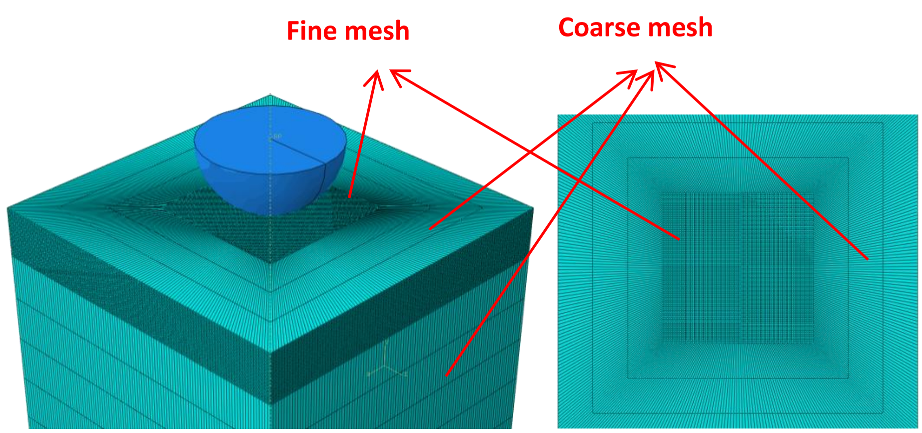


Figure 4.3: Shows the mesh of the target material of region-1, where the fine mesh has been done and region-2, where coarse mesh has been done.

## 4.6 Boundary Condition in SMAT Modeling

In figure 4.4 shows the boundary condition of the finite element model for the single impact. In this model, the bottom surface of the target is fully fixed/ encastre (U1=U2=U3=UR1=UR2=UR3=0) and the center of the shot is fixed in all the direction except U2 direction (U1=U3=UR1=UR2=UR3=0, U2≠ **0**).

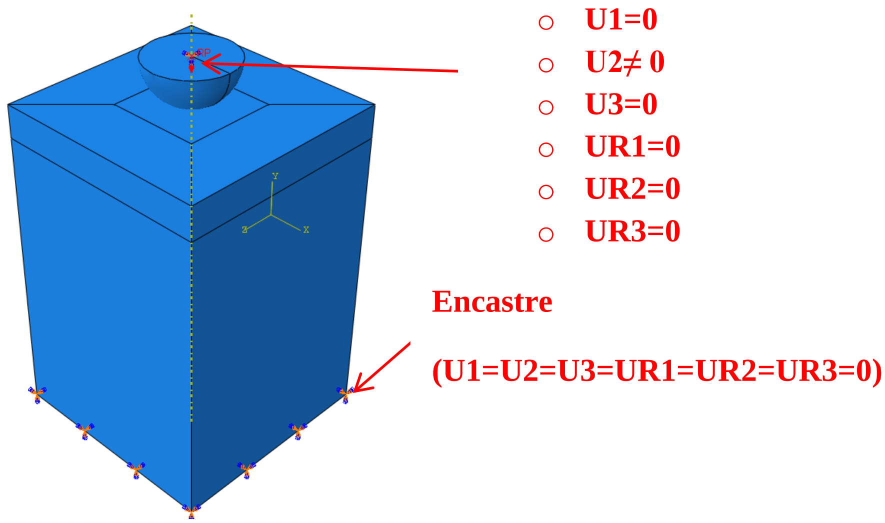


Figure 4.4: Shows the boundary conditions of the Finite Element model with some predefined velocity of the shot.

## 4.8 Numerical Model of Single Point Multiple Impact SMAT

In this single point multiple impact model, 3, 5, and 7 shot/ ball was used, which is shown in fig.4.5. SMAT is a process where the shot was impacted multiple times at the same point on the target; this number of impact depends on the SMAT time. To see the effect of multiple impacts at the same point single point multiple impact model was developed.

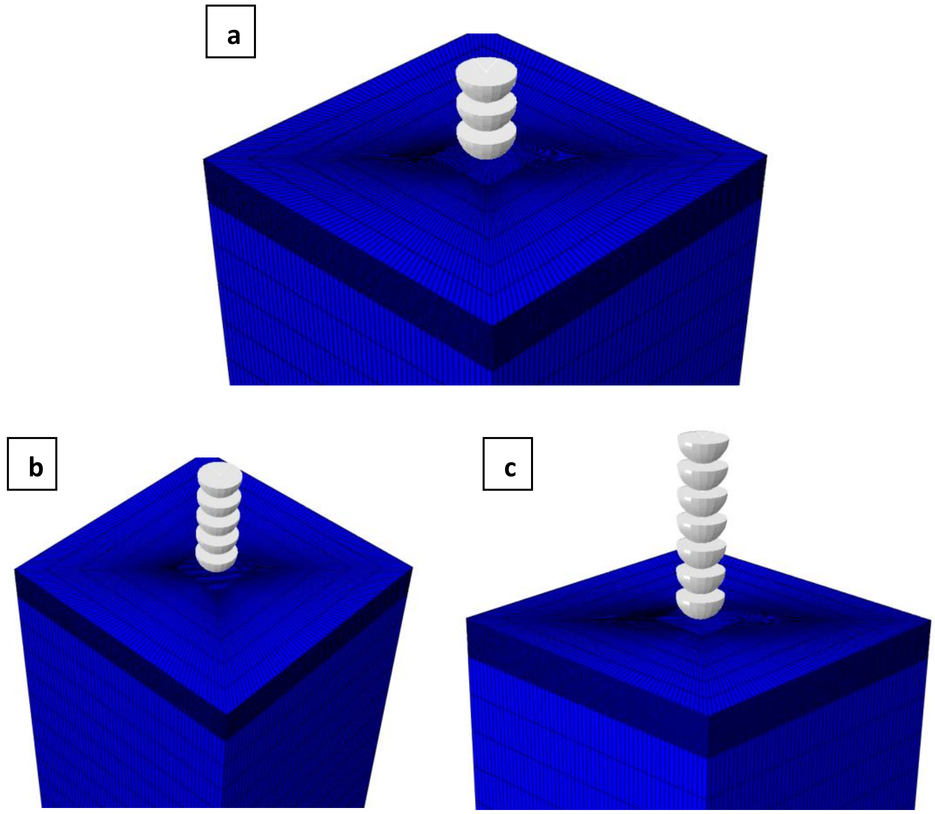


Figure 4.5: Finite elements model for single point multiple impact SMAT (a) single point 3 impact model (b) single point 5 impact model (c) single point 7 impact model.

## 4.9 Numerical Model of Multiple Points Multiple Impacts SMAT

The idea for developing the multiple points multiple impact models to investigate the simulated results from the actual experimental result, for this we developed a Python script which can run in ABAQUS EXPLICIT 6.14. In this python script, we developed code for random coordinates of the shot and also for the random shot velocity.

Since shot impact in SMAT has intrinsic random characteristics, a random sequence of shots must be taken into account for numerical modeling of multiple impacts. ABAQUS scripting using Python programming language was utilized to build multiple points multiple impact model.

## 4.10 Stress and PEEQ Contour Plot of Smated Sample

Figure 4.6 shows the stress and plastic strain contour plot along with the depth of the sample and on the surface of the SMATed sample by using 5mm shot diameter and 1 m/s shot velocity. Fig. 4.6 (a) and (b) shows the stress distribution of the SMATed sample along with the depth and on the surface respectively. Fig 4.6 (c) and (d) shows the PEEQ distribution of the SMATed sample along with the depth and on the surface respectively. Path-1(along with the depth) and path-2 (distance from the center of impact) were created to study the effect of SMAT on these two paths.

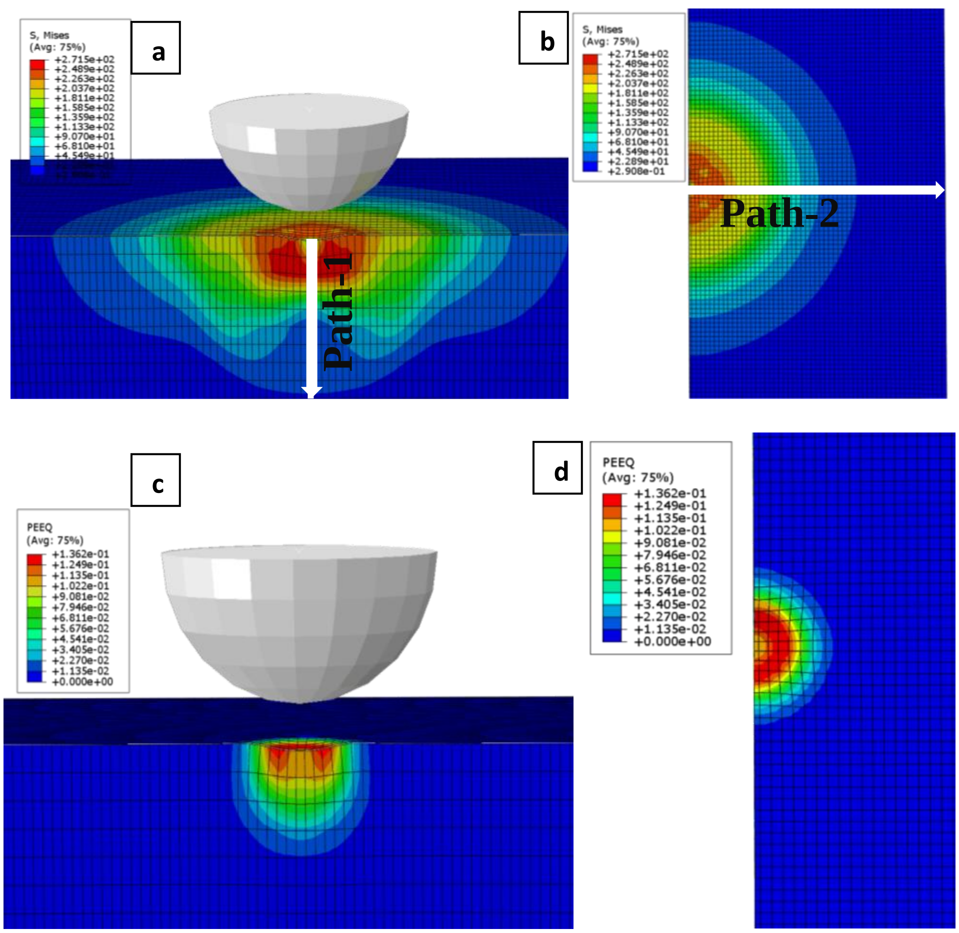


Figure 4.6: Stress contour plot (a) global view (b) top view and PEEQ contour plot (c) global view (d) top view of single impact SMATed material.

# CHAPTER 5

# RESULT AND DISCUSSION

In this chapter, results are shown in the form of contour plots and 2D curves, to better understand the parameter such as equivalent plastic strain (PEEQ), compressive residual stresses, equivalent residual stresses (EQRS) and the displacement of the surface for the SMAT, single point single impact, single point multiple impacts, and multiple points multiple impacts processes. The effect of size of the shot and impact velocity was also studied in this work. For this purpose, the size of the shot was varied from 3 mm to 8 mm and impact velocity was varied from 1 m/s to 15 m/s.

## 5.1 Single Point Single Impact Results

In this section, numerical simulation of single point single impact result is presented with different SMAT process parameter. Fig. 5.1 shows the top view and in-depth distribution of parameters, such as equivalent plastic strain (PEEQ) and equivalent residual stress after a single impact with 3 mm diameter shot and 5 m/s impact velocity. As shown in fig. 5.1(a) the maximum PEEQ value is 0.382 which is not at the center of impact but in the location near the center. This phenomenon can be understood using the Hertz contact theory. According to this theory, the depth of the maximum shear stress is dependent on the size of the contact region [45]. Fig 5.1 (b) shows the maximum PEEQ value is not at the surface of impact, but slightly below it. Maximum EQRS developed after a single impact was 360 MPa as shown in fig. 5.1 (c, d). The maximum EQRS is found at the location near the center of impact also in-depth, the location of the maximum EQRS value is not at the impact surface, but slightly below the treated surface.

Fig. 5.2 shows the result along with the two paths, of single point single impact for different impact velocity with 3 mm shot. Fig. 5.2 (a, b) shows the variation of equivalent plastic strain (PEEQ) along with the depth and along the surface path passing through the center of impact respectively.  It can be seen that from figure 5.2(a.b) with increase in impact velocity the value of PEEQ was also increased for both the paths.

Fig.5.2 (c) shows the variation of compressive residual stress (CRS) along with the depth of the SMAted sample after single impact for different impact velocity with 3 mm shot diameter. It can be seen from the fig 5.2(c) the maximum compressive residual stress (CRS) is increasing when increasing the impact velocity. Maximum CRS in case of 1 m/s impact velocity is -119.205 MPa and for 15m/s impact velocity the value of maximum CRS is -227.83 MPa. It can be seen from fig. 5.2(d) the maximum displacement in the direction of impact is increased with increase of the impact velocity. The vertical displacement is increased from 0.06896 mm to 0.9804 mm for the impact velocity increased from 1 m/s to 15 m/s. The vertical displacement is followed as the result of the permanent plastic deformation generated due to the impact loading. Due to such impact, the kinetic energy (KE) of the shot was transformed into the potential energy (PE) stored in the treated material in the form of plastic deformation, phase transformation twinning, etc. After the analysis of these results shows the impact velocity of the shot has a significant influence on the generation of PEEQ, CRS, and the deformation of the material.

After the study, the influence of the impact velocity of the shot on the treated material, the influence of shot diameter were studied. For this study, three different sizes of the shot 3 mm, 5 mm, and 8 mm were taken with 1 m/s constant impact velocity. Fig.5.3 represents the variation of the PEEQ for both the paths, CRS along with the depth, and vertical displacement of the surface, for the single point single impact. From the fig 5.3(a, b) it can be seen that with increase in the shot diameter the value of maximum PEEQ is also increased for both the paths and also seen that the thickness of the PEEQ layer for 0.2% PEEQ along with the depth is significantly increased from 0.2368 mm to 0.6279 mm for the shot diameter increased from 3 mm to 8 mm. Fig. 5.3 (c) shows the distribution of compressive residual stress (CRS) along with the depth of the treated surface for different shot diameter. It can be seen that from this figure the value of the maximum CRS is increasing with increasing of the shot diameter and also the thickness of the CRS layer along with the depth is increasing. Maximum CRS in case of 3 mm shot diameter is -119.205 MPa and for 8 mm shot diameter the value of maximum CRS is -184.542 MPa. Fig 5.3 (d) shows the distribution of the vertical displacement of the surface. It can be seen from the figure the vertical displacement of the surface is increasing with increasing the diameter of the shot. Maximum vertical displacement in case of 3 mm shot diameter is 0.06896 mm and for 8 mm shot diameter is 0.1939 mm.

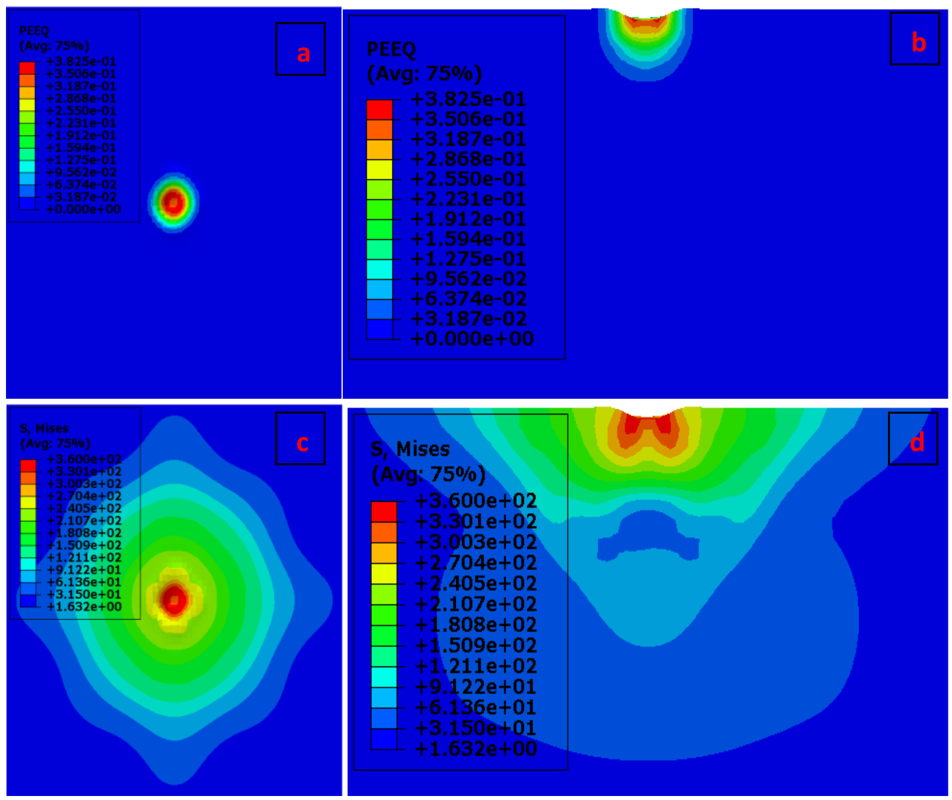


Figure 5.1: Distribution of equivalent plastic strain (PEEQ) (a) top view (b) in depth, and equivalent residual stress (EQRS) (MPa) (c) top view (d) in depth, after single impact with 3 mm shot and 5 m/s impact velocity.

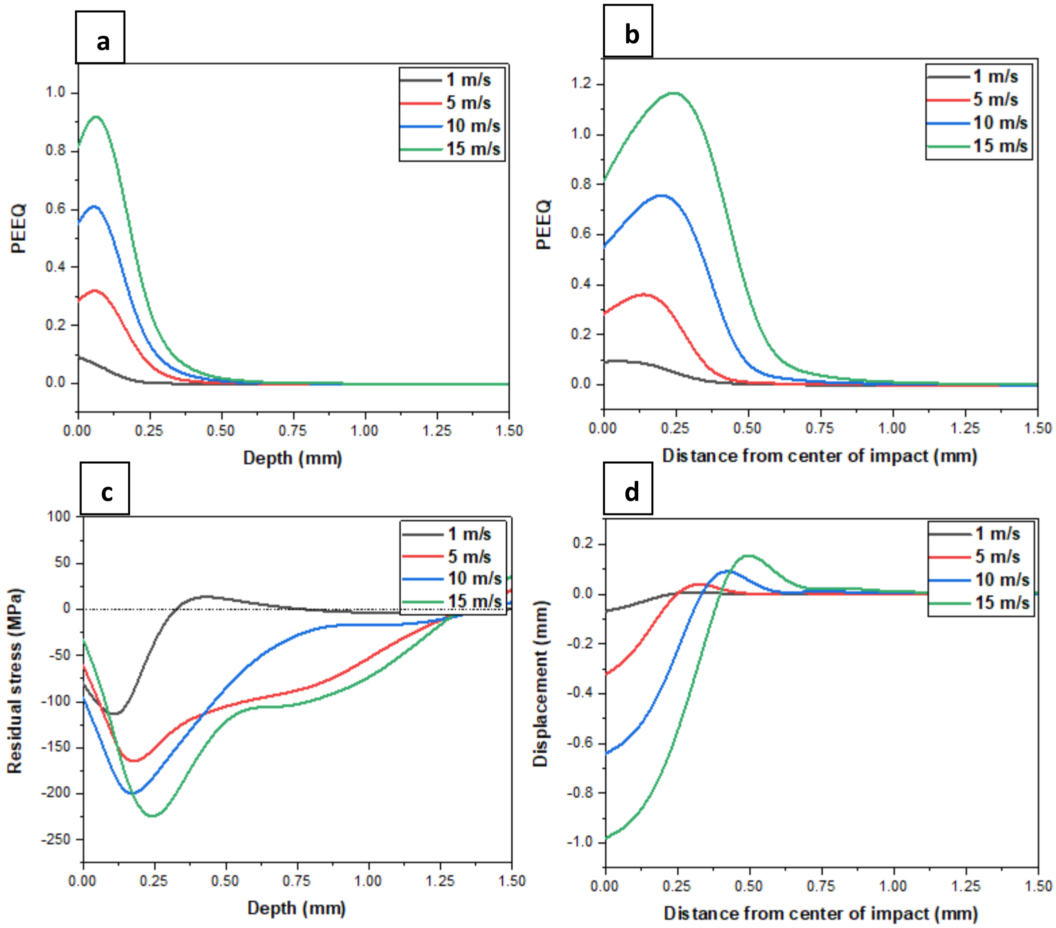


Figure 5.2: Variation of equivalent plastic strain (PEEQ) (a) along with the depth, (b) along the surface path passing through the center of impact, (c) residual stress along the depth, and (d) displacement along the surface path passing through the center of impact, after the single impact with 3 mm shot and different impact velocity.

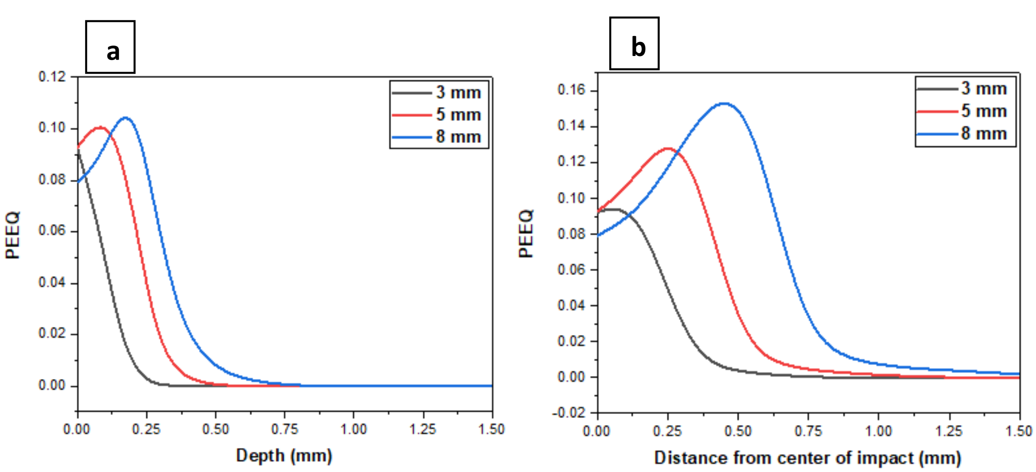

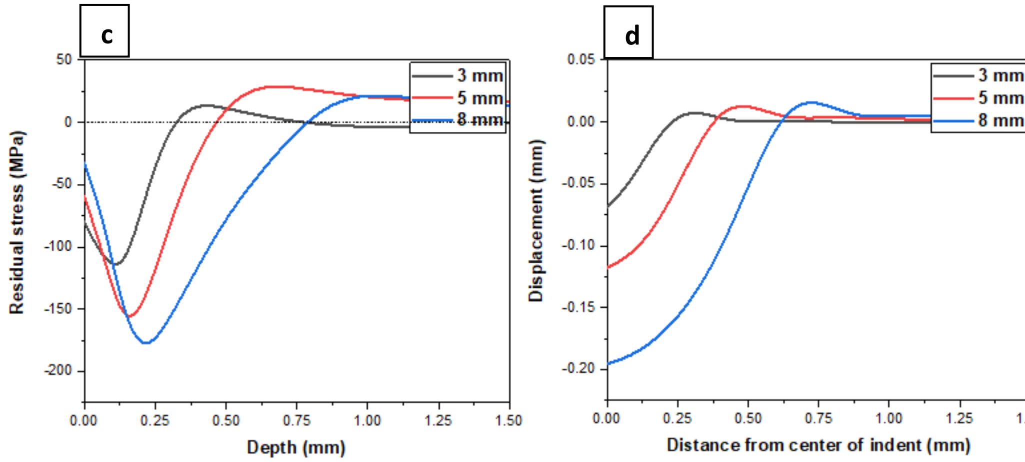


Figure 5.3: Variation of equivalent plastic strain (PEEQ) (a) along with the depth, (b) along the surface path passing through the center of impact, (c) residual stress along the depth, and (d) displacement along the surface path passing through the center of impact, after the single impact with 1m/s impact velocity and different shot diameter velocity.

It can be seen the effect of 5 mm and 8 mm shot in the variation of the PEEQ for both the paths, CRS along with with the depth, and vertical displacement of the surface with different velocity, for the single point single impact in fig. 5.4. Fig. 5.4 (a) and 5.5 (a) shows the distribution of PEEQ along with the depth of treated material. It can be observed that in the case of 5 mm shot, PEEQ increases from 0.0975 to 0.7564 and for 8 mm shot it increases from 0.1017 to 0.8737 with an increment of velocity from 1 m/s to 15 m/s. Fig 5.4(b) and fig. (b) Shows the distribution of the PEEQ along the treated surface for 5 mm shot and 8 mm shot. Fig 5.4 (c) and fig. 5.5 (c) shows the distribution of CRS for 5 mm shot and 8 mm shot. For 5 mm shot, the maximum CRS value increase from -161.221 MPa to -307.915 MPa and for 8 mm shot the maximum CRS value increases from -179.176 MPa to -205.649 MPa when increasing the impact velocity from 1 m/s to 5 m/s. Fig. 5.4(d) and fig. 5.5(d) shows the distribution of vertical displacement of the treated surface for a single impact. From this figure, it can be seen that vertical displacement is increasing with the increase in impact velocity. In the case of 5 mm and 8 mm shot the maximum vertical displacement changes from 0.1211 mm to

1.72884 mm and from 0.19618 mm to 2.9597 mm respectively when increasing the velocity 1 m/s to 5 m/s.

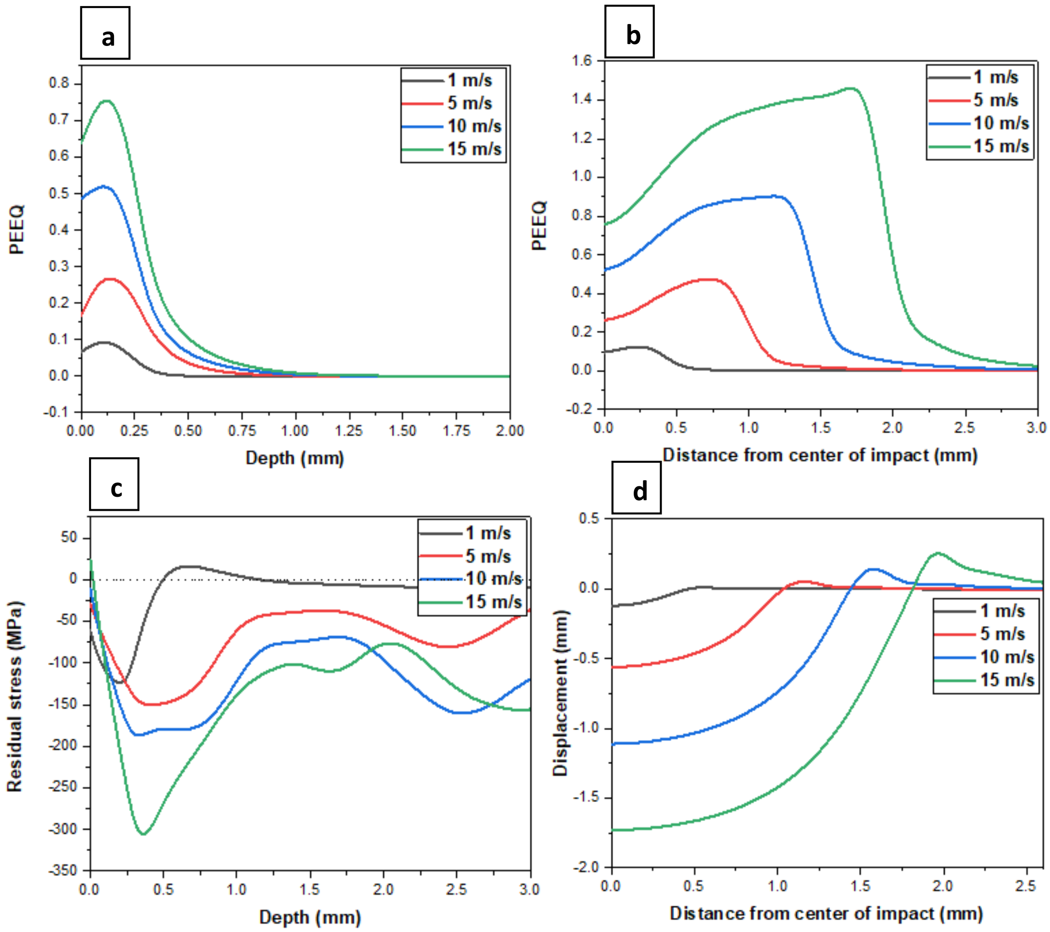


Figure 5.4: Variation of equivalent plastic strain (PEEQ) (a) along with the depth, (b) along the surface path passing through the center of impact, (c) residual stress along the depth, and (d) displacement along the surface path passing through the center of impact, after the single impact with 5 mm shot and different impact velocity.

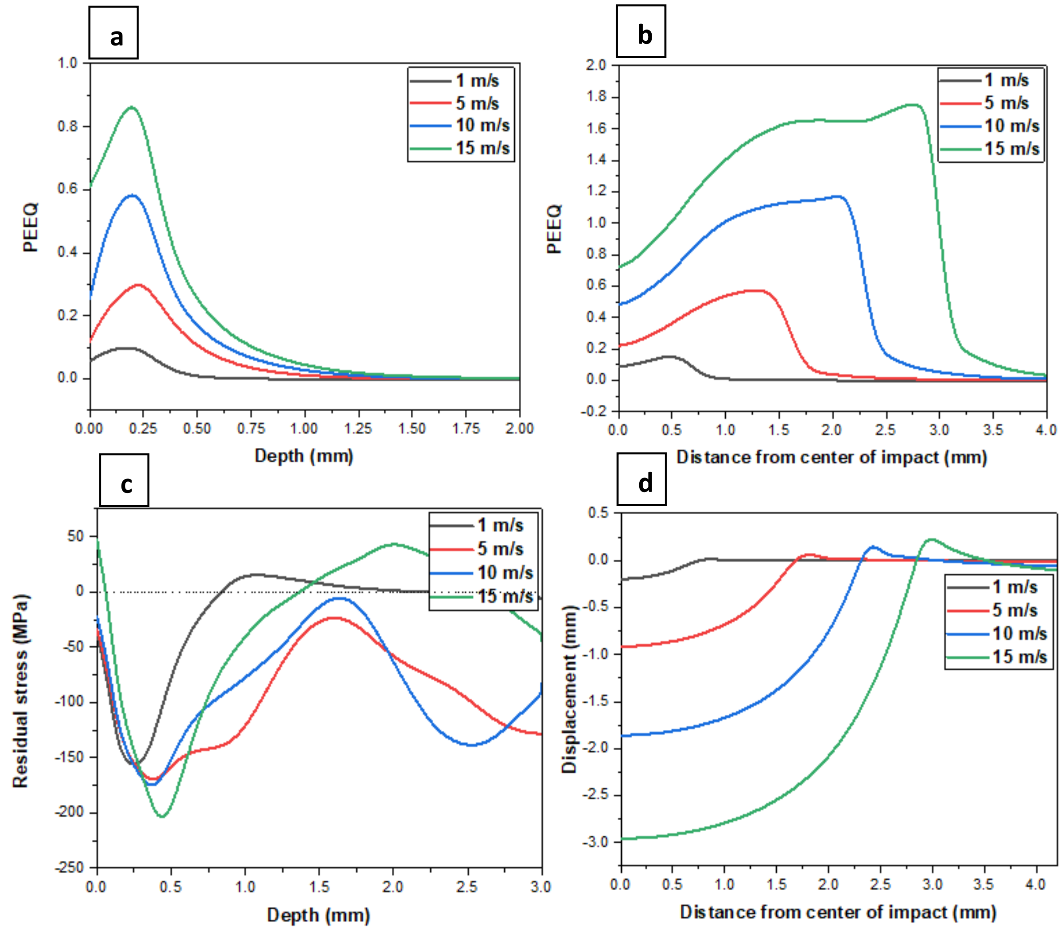


Figure 5.5: Variation of equivalent plastic strain (PEEQ) (a) along with the depth, (b) along the surface path passing through the center of impact, (c) residual stress along the depth, and (d) displacement along the surface path passing through the center of impact, after the single impact with 8 mm shot and different impact velocity.

The indent diameter and indent depth developed after a single impact are significantly affected by the SMAT process parameter i.e. the size of the shot and the impact velocity. Fig 5.6 (a) shows the relationship between the indent depth size and SMAT process parameter ( size of the shot and impact velocity ). It can be seen that from this figure the indent depth size has a linear relation with impact velocity for all three shot diameter (3 mm, 5 mm, and 8 mm ).

Fig. 5.6 (b) shows the relationship between the indent diameter size and SMAT process parameter ( size of the shot and impact velocity ). It can be seen that from this figure the indent diameter size has a linear relation with impact velocity for all three shot diameter (3 mm, 5 mm, and 8 mm ). It has already seen that during a literature survey, Kirk and Iida provided the linear relation between indent diameter size vs. impact velocity and indent depth size vs impact velocity for single impact [30].

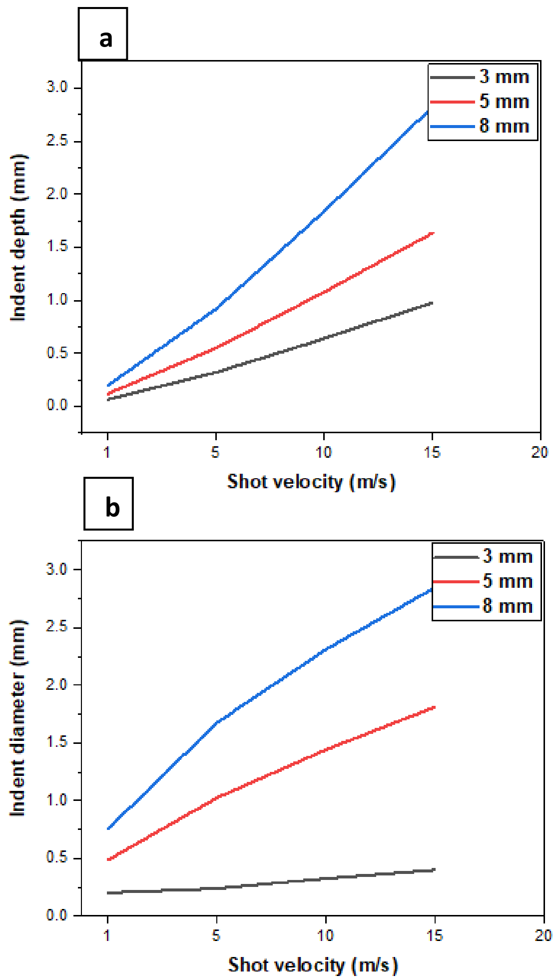


Figure 5.6: Analysis of the effects of SMAT parameters (size of the shot and impact velocity) on (a) the indent depth size, and (b) indent diameter size.

## 4.2 Single Point Multiple Directions Impact Results

Fig. 5.7 shows the top view and in-depth contour plots of equivalent residual stress (MPa) single 3 mm shot impacted with velocity 5 m/s from different directions.

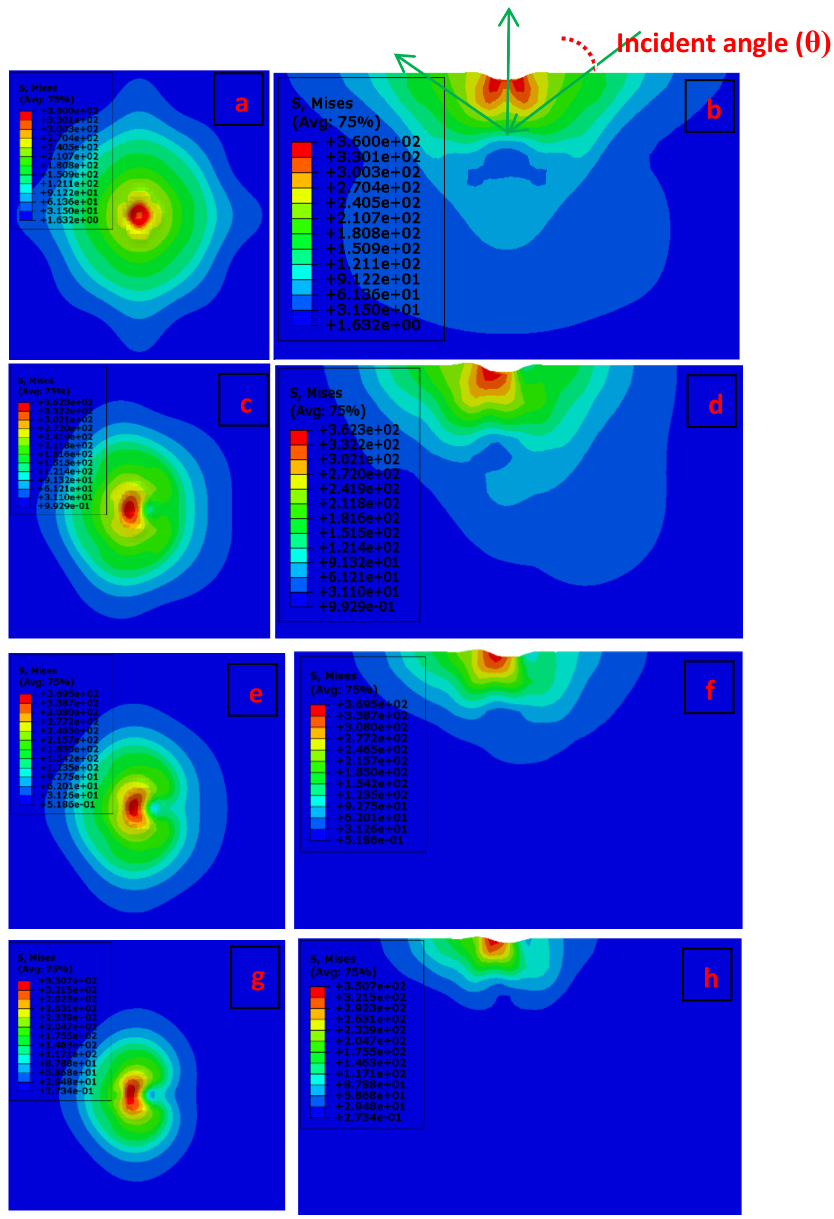


Figure 5.7: Top view and in-depth distribution of equivalent residual stress (MPa) for (a, b) $90^0$ of impact angle, (c, d) $60^0$ of impact angle, (e, f) $45^0$ of impact angle, and (g, h) $30^0$ of impact angle, for 3 mm shot and 5 m/s impact velocity.

As shown in fig. 5.7 the impact velocity of the shot is 5 m/s with incident angle θ ( θ = $90^0$, $60^0$, $45^0$, and $30^0$ ) was used in this case. So the impact velocity coordinate was $v_x = v \cos\theta$, $v_y = v \sin\theta$ and $v_z = 0$. The equivalent residual stress after a single impact from a different direction is compared in this fig. 5.7. It can be seen from this figure the equivalent residual stress is not symmetric about the center line and also the depth of the equivalent residual stress is decreasing with decreasing angle of incident. From fig. 5.8 (a) it can see that the PEEQ along with the depth is maximum for $60^0$ incident angle and for $30^0$ incident angle it is minimum. Fig. 5.8 (b) for $60^0$ and $30^0$ incident angle the value of maximum PEEQ is almost the same about 0.42 and for $45^0$ it is maximum about 0.46326. Fig. 5.8 (c) shows the distribution of compressive residual stress for various shot incident angles. It can be seen from the figure maximum value of CRS is increasing with decreasing the incident angle. For $90^0$ maximum value of CRS is -205.177 MPa and for $30^0$ is -52.7378 MPa. Fig. 5.8 (d) shows that the vertical displacement of the surface is not symmetric about the center line and also the vertical displacement is decreasing with decreasing angle of incident. In the case of $90^0$ incident angle and $30^0$ incident angle shot the maximum vertical displacement changes from 0.323066 mm to 0.152276 mm.

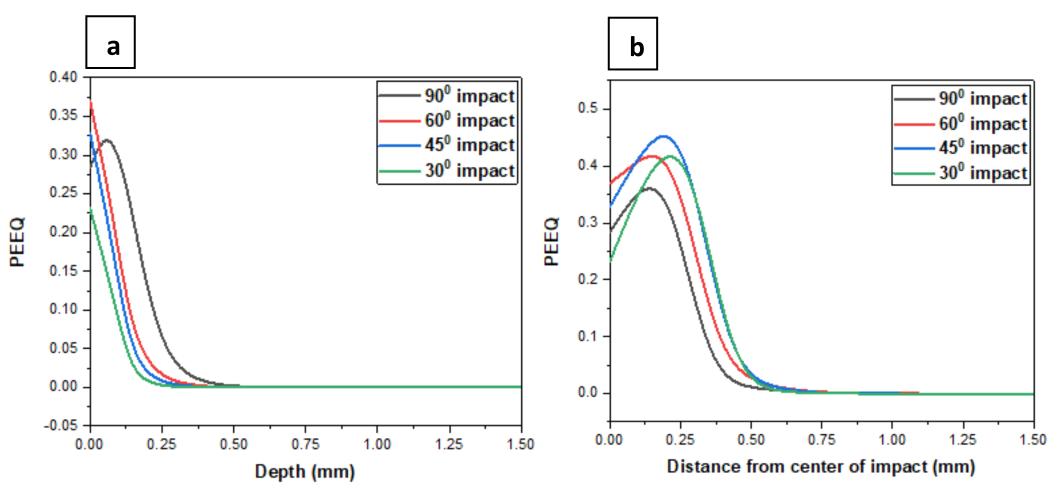

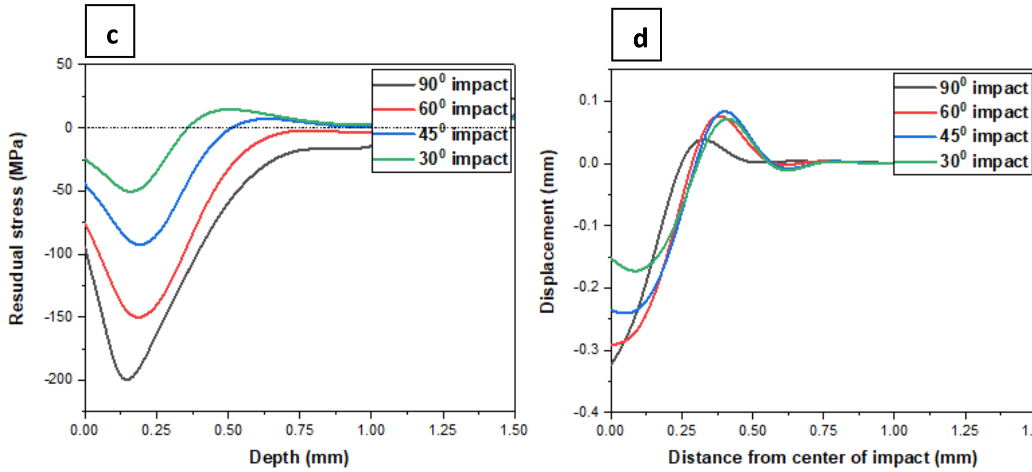


Figure 5.8: Variation of equivalent plastic strain (PEEQ) (a) along with the depth, (b) along the surface path passing through the center of impact, (c) residual stress along the depth, and (d) displacement along the surface path passing through the center of impact, after the single impact with 3 mm shot and 5 m/s impact velocity for different impact angle.

## 4.3 Single Point Multiple Impact Results

In this section, single point multiple impact simulations have been done to see the effect for successive impact on the material. Fig. 5.9 show the contour plot of Evolution of PEEQ in the impacting process with 1, 3, 5, and 7 shot. It can be seen from this figure depth of the plastic zone size is increasing with increasing the number of shot and also the size of the plastic zone size on the surface is increasing. Fig. 5.10 (a, b) shows the distribution of PEEQ along with the depth and along the surface of the treated material. Fig. 5.10 (c) shows the CRS distribution for different shot impact on the material. The maximum CRS value is increasing with increasing the shot impact. Fig. 5.10 (d) shows the distribution of vertical displacement of a different number of the impact of the shot. The vertical displacement increasing from 0.323066 mm to 0.858067 mm when the number of shot is increasing from 1 to 7.

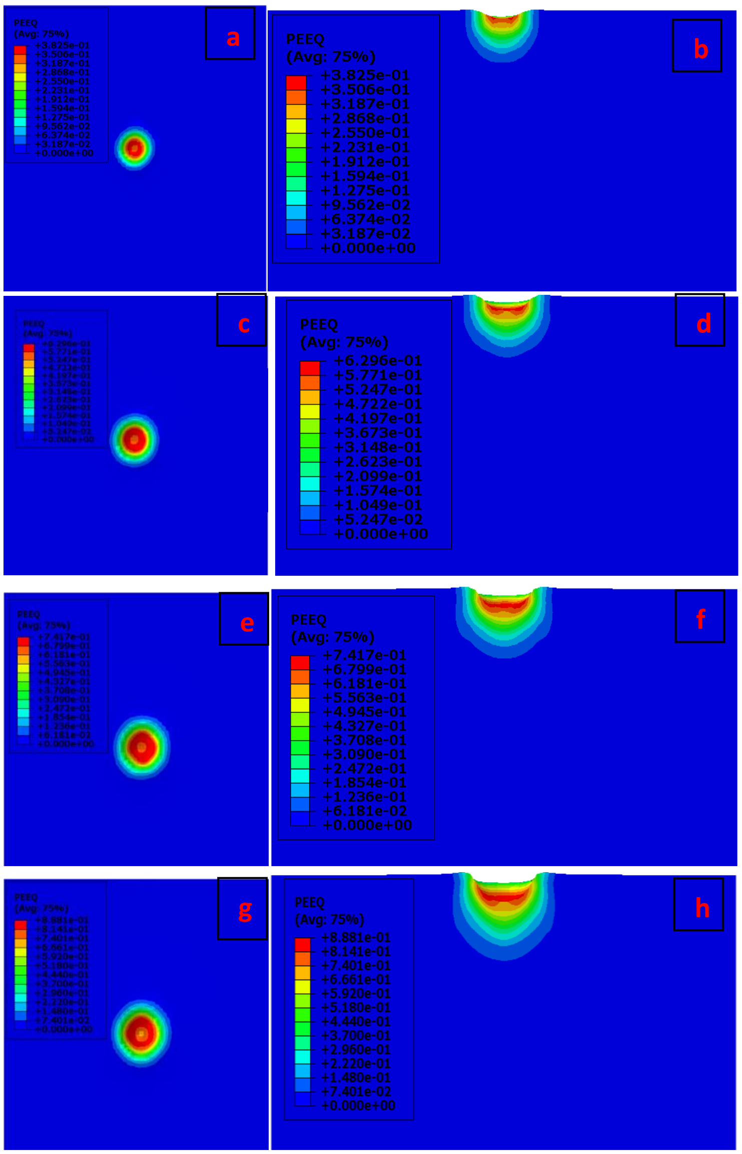


Figure 5.9: Top view and in-depth distribution of equivalent plastic strain (PEEQ) for (a,b) single point single impact, (c,d) single point 3 times impact, (e,f) single point 5 times impact, and (g,h) single point 7 times impact, for 3 mm shot and 5 m/s impact velocity.

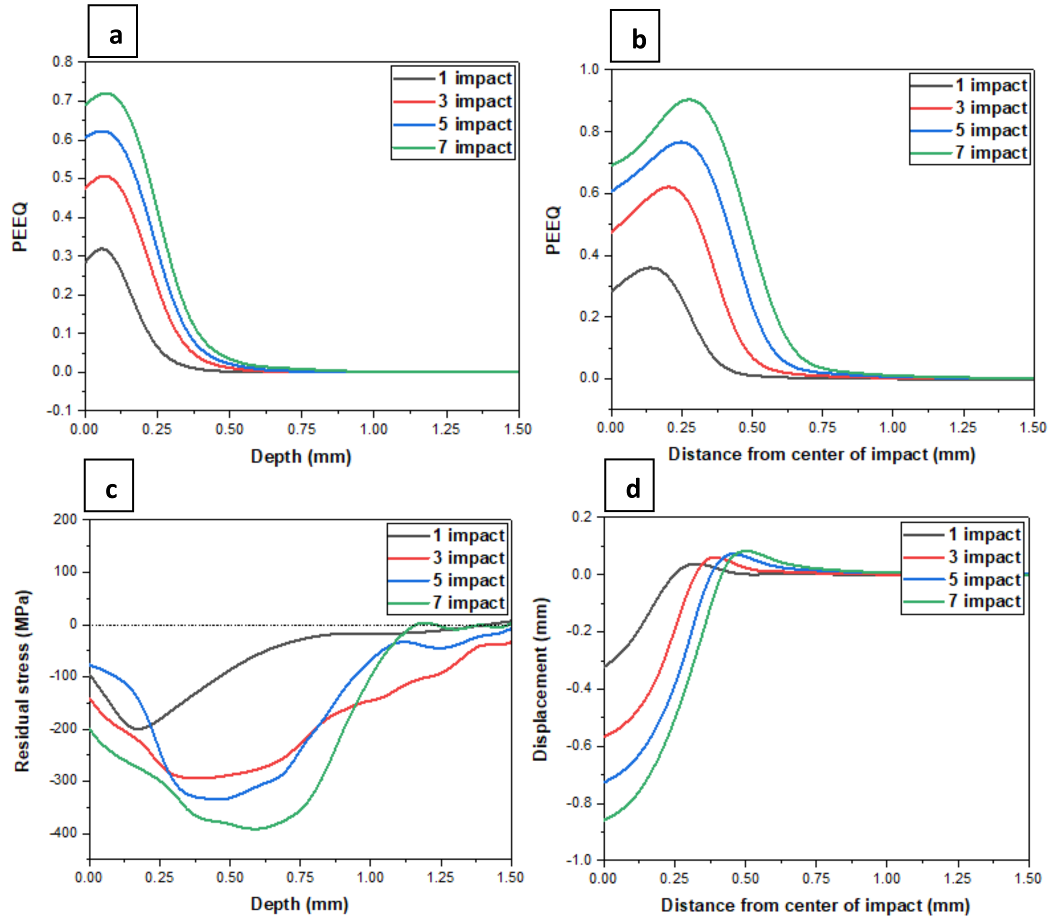


Figure 5.10: Variation of equivalent plastic strain (PEEQ) (a) along with the depth, (b) along the surface path passing through the center of impact, (c) residual stress along the depth, and (d) displacement along the surface path passing through the center of impact, after the single impact with 3 mm shot and 5 m/s impact velocity for single point multiple impacts.

The indent diameter and indent depth developed after a single impact as well as multi-impact are significantly affected by the SMAT process parameter i.e. the size of the shot and the impact velocity. Fig 5.6 (a) shows the relationship between the indent depth size and SMAT process parameter (impact velocity ). It can be seen that from this figure the indent depth size has a decreasing order of parabolic relation with impact velocity for the different impact of shot (1, 3, 5, and 7 ).

Fig. 5.6 (b) shows the relationship between the indent diameter size and SMAT process parameter ( impact velocity ). In this case, also it can be seen that from this figure the indent diameter size has a decreasing order of parabolic relation with impact velocity for the different impact of shot (1, 3, 5, and 7 ).

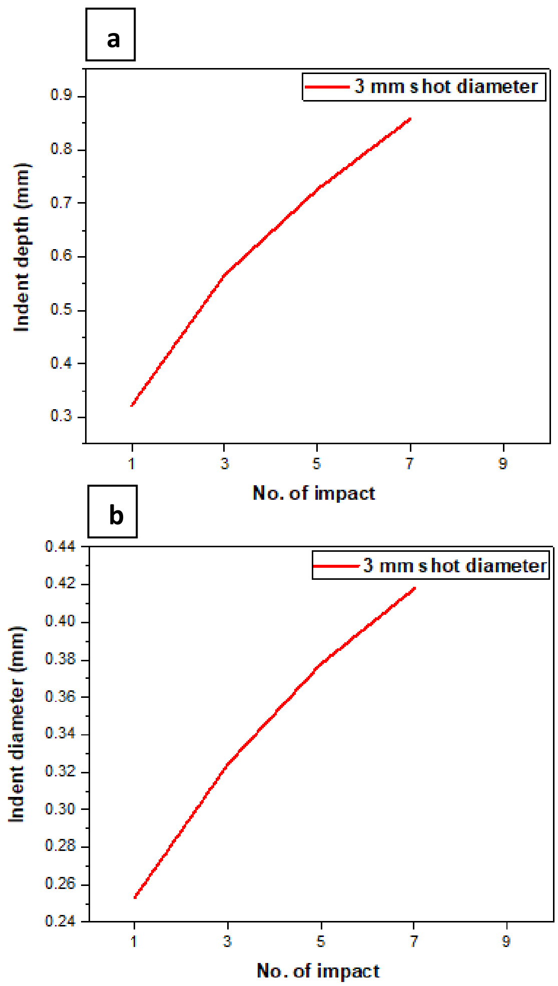


Figure 5.11: Analysis of the effects of multiple impacts on a single point on (a) the indent depth size, and (b) indent diameter size, with 3 mm shot and 5 m/s impact velocity.

## 4.3 Multiple Point Multiple Impact Results

The idea for developing the multiple points multiple impact models to investigate the simulated results from the actual experimental result, for this we developed a Python script in which code has been developed for random coordinates of the shot and also for the random shot velocity.

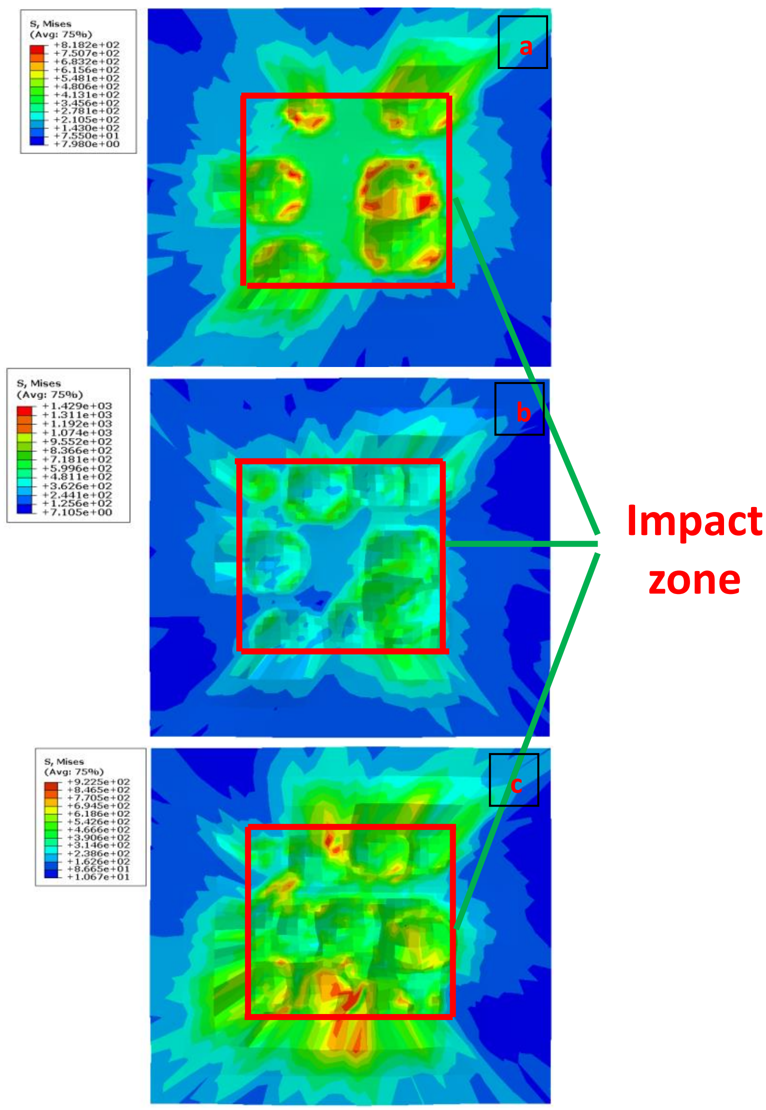


Figure 5.12: Evaluations of coverage (a) 25% coverage, (b) 50% coverage, and (c) 100% coverage, for SMAT process: finite element Simulation results for the random impact model by using 4 mm shot diameter with random impact velocity.

Fig. 1.12 show the evolution of 100% coverage for the SMAT process using 4 mm shot diameter with random impact velocity in the range of 1 m/s to 15 m/s. during the simulation it has been observed that 32 times a shot were impacted on the impact zone to cover all 100% area. Fig. 5.13 (a) shows that, the PEEQ variation along with the depth for 100% coverage. It can be seen that from this figure the PEEQ is maximum at the surface and it is decreasing along with the depth [32]. shows that, the CRS variation along with the depth for 100% coverage.

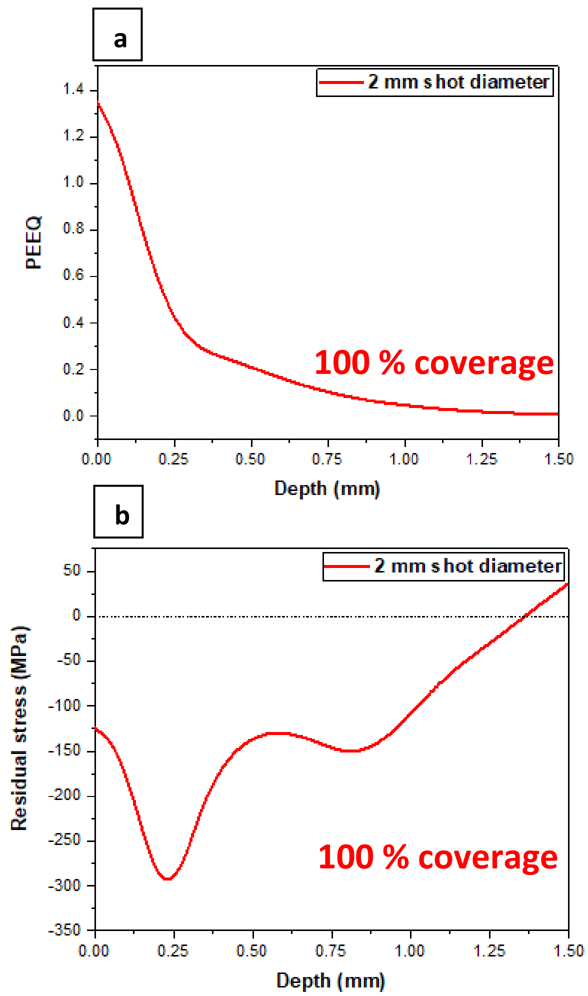


Figure 5.13: Variation of (a) equivalent plastic strain (PEEQ), (b) residual stress, along with the depth SMAted with 2 mm shot for 100 % coverage

# CHAPTER 6

## CONCLUSIONS

In this study, three-dimensional finite element models of single shot impact and multiple shot impacts are developed to see the effect of the SMAT process parameter. The residual equivalent stress (EQRS), the compressive residual stress (CRS), the equivalent plastic strain (PEEQ), the permanent plastic deformation (vertical displacement) after a single impact were analyzed. Analyzed the effect on the equivalent plastic strain (PEEQ), vertical displacement of the treated surface, and the compressive residual stress (CRS) for multiple impacts at the same point. The equivalent plastic strain (PEEQ) and the compressive residual stress (CRS) for 100% coverage.

- It has been found that with the increasing impact velocity the maximum compressive residual stress (CRS), the equivalent plastic strain (PEEQ), indent diameter size and indent depth size is increasing.
- With increasing size of the shot the maximum CRS, PEEQ, indent diameter size and indent depth size is increasing. In this case, depth (thickness) of the compressive residual stress layer is also increasing.
- The indent diameter and indent depth developed after a multi-impact are significantly affected by the SMAT process parameter i.e. the size of the shot and the impact velocity. With an increasing number of impacts the PEEQ, indent diameter, and indent depth are increasing.
- It has been that evaluations of coverage for the random impact model by using 4 mm shot diameter with random (1-15 m/s) impact velocity.

# REFERENCES


[1.] Altenberger, I., Scholtes, B., Martin, U. and Oettel, H. (1999), Cyclic deformation and near surface microstructures of shot peened or deep rolled austenitic stainless steel AISI 304, Materials Science and Engineering: A, 264, 1–16.

[2] Jian Lu, K.Lu, Generation of Nanostructure by SMAT basic concepts, different processes, and applications, Alternative Processes, 163-170.

[3] N.R. Tao, M.L. Sui, J. Lu, K. Lua, Surface nanocrystallization of iron-induced by ultra-sonic shot peening, nanostructure, mater,11 (1991).

[4] H.W. Zhang, Z.K. Hei, G. Liu, J. Lu, K. Lu, Formation of the nanostructured surface layer on AISI 304 stainless steel by means of surface mechanical attrition treatment, Acta Mater. 51 (2003) 1871–1881, http://dx.doi.org/10.1016/S1359-6454(02)00594-3.

[5] X. Wu, N. Tao, Y. Hong, B. Xu, J. Lu, K. Lu, Microstructure and evolution of mechanically-induced ultrafine grain in surface layer of AL-alloy subjected to USSP, Acta Mater. 50 (2002) 2075–2084, http://dx.doi.org/10.1016/S1359-6454(02)00051-4.

[6] Z. Yin, X. Yang, X. Ma, J. Moering, J. Yang, Y. Gong, Y. Zhu, X. Zhu, Strength and ductility of gradient structured copper obtained by surface mechanical attrition treatment,Mater.

[7] Zhang, H.W., Hei, Z.K., Liu, G., Lu, J., Lu, K., 2003. Formation of nanostructured surface layer on AISI 304 stainless steel by means of surface mechanical attrition treatment. Acta Mater. 51, 1871–1881.

[8] N.R. Tao, Z.B. Wang, W.P. Tong, M.L. Sui, J. Lu, K. Lu, An investigation of surface nanocrystallization mechanism in Fe induced by surface mechanical attrition treatment, Acta Mater. 50 (2002) 4603–4616, http://dx.doi.org/10.1016/S1359-6454(02)00310-5.

[9] DAI, K., & SHAW, L. (2008). *Analysis of fatigue resistance improvements via surface severe plastic deformation. International Journal of Fatigue, 30(8), 1398–1408.*doi:10.1016/j.ijfatigue.2007.10.010

[10] Menezes, M. R., Godoy, C., Buono, V. T. L., Schvartzman, M. M. M., & Avelar-Batista Wilson, J. C. (2017). Effect of shot peening and treatment temperature on wear and corrosion resistance of sequentially plasma treated AISI 316L steel. Surface and Coatings Technology, 309, 651–662. doi:10.1016/j.surfcoat.2016.12.037

[11] Arifvianto, B., Suyitno, Mahardika, M., Dewo, P., Iswanto, P. T., & Salim, U. A. (2011). *Effect of surface mechanical attrition treatment (SMAT) on microhardness, surface roughness and wettability of AISI 316L. Materials Chemistry and Physics, 125(3), 418–426.*doi:10.1016/j.matchemphys.2010.10.038

[12] Tao, N., Zhang, H., Lu, J., Lu, K., 2003. Development of nanostructures in metallic materials with low stacking fault energies during surface mechanical attrition treatment (SMAT). Mater. Trans. 44, 1919–1925

[13] Priestner, R., & Priestner, D. M. (1991). Importance of Substrate in Surface Engineering. Surface Engineering, 7(1), 53 60.doi:10.1179/sur.1991.7.1.53

[14] Wierzchon T. Burakowski T. Surface engineering of metals: Principles, equipment, technologies. 199

[15] A Q Lu¨, Y Zhang, Y Li, G Liu, Q H Zang, and C M Liu. Effect of nanocrystalline and twin boundaries on corrosion behavior of 316L stainless steel using SMAT. Acta Metallurgica Sinica (English Letters), 19(3):183–189, 2006

[16] H Lee, D Kim, J Jung, Y Pyoun, and K Shin. Influence of peening on the corrosion properties of AISI 304 stainless steel. Corrosion Science, 51(12):2826–2830, 2009

[17] Roland Bryon Heywood. Designing against fatigue of metals. Reinhold, 1962.

[18]Maleki, E., Unal, O., & Kashyzadeh, K. R. (2018). *Effects of conventional, severe, over, and re-shot peening processes on the fatigue behavior of mild carbon steel. Surface and Coatings Technology, 344, 62–74.*doi:10.1016/j.surfcoat.2018.02.081

[19] Mohseni, E., Zalnezhad, E., Sarhan, A. A. D., & Bushroa, A. R. (2014). A Study on Surface Modification of Al7075-T6 Alloy against Fretting Fatigue Phenomenon. Advances in Materials Science and Engineering, 2014, 1–17. doi:10.1155/2014/474723

[20] Kubler, R. F., Berveiller, S., Bouscaud, D., Guiheux, R., Patoor, E., & Puydt, Q. (2019). Shot peening of TRIP780 steel: experimental analysis and numerical simulation. Journal of Materials Processing Technology.doi:10.1016/j.jmatprotec.2019.02.031

[21] J Azadmanjiri, C C Berndt, A Kapoor, and C Wen. Development of surface nanocrystallization in alloys by surface mechanical attrition treatment (SMAT). Critical Reviews in Solid State and Materials Sciences, 40(3):164–181, 2015.

[22] N Hansen, R F Mehl, et al. New discoveries in deformed metals. Metallurgical and materials transactions A, 32(12):2917–2935, 2001

[23] Gatey, A. M., Hosmani, S. S., & Singh, R. P. (2015). Surface mechanical attrition treated AISI 304L steel: role of process parameters. Surface Engineering, 32(1), 69–78.doi:10.1179/1743294415y.000000005

[24] Wang, Z.B., Tao, N.R., Li, S., Wang, W., Liu, G., Lu, J. and Lu, K. (2003c), Effect of surface nanocrystallization on friction and wear properties in low carbon steel, Materials Science and Engineering: A, 352, 144–149.

[25] Zhang, Y.S., Han, Z. and Lu, K. (2008), Fretting wear behavior of nanocrystalline surface layer of copper under dry condition, Wear, 265, 396–401.

[26] Anand Kumar, S., Ganesh Sundara Raman, S., Sankara Narayanan. T.S.N. and Gnanamoorthy, R. (2013), Influence of counter body material on fretting wear behavior of surface mechanical attrition treated Ti–6Al–4V, Tribology International, 57, 107–114

[27] Kalsar, R., & Suwas, S. (2018). A novel way to enhance the strength of twinning induced plasticity (TWIP) steels. Scripta Materialia, 154, 207–211.doi:10.1016/j.scriptamat.2018.05.045

[28] Chen, X.H., Lu, J., Lu, L. and Lu, K. (2005), Tensile properties of a nanocrystalline 316L austenitic stainless steel, Scripta Materialia, 52, 1039–1044.

[29] Roland, T., Retraint, D., Lu, K., & Lu, J. (2006). Fatigue life improvement through surface nanostructuring of stainless steel by means of surface mechanical attrition treatment. Scripta Materialia, 54(11), 1949–1954.doi:10.1016/j.scriptamat.2006.01.049

[30] Li, D., Chen, H.N. and Xu, H. (2009), The effect of nanostructured surface layer on the fatigue behaviors of a carbon steel, Applied Surface Science, 255, 3811–3816.

[31] Mao, X. Y., Li, D. Y., Fang, F., Tan, R. S., & Jiang, J. Q. (2011). Application of a simple surface nanocrystallization process to a Cu–30Ni alloy for enhanced resistances to wear and corrosive wear. Wear, 271(9-10), 1224–1230.doi:10.1016/j.wear.2010.12.063

[32] Heydari Astaraee, A., Miresmaeili, R., Bagherifard, S., Guagliano, M., & Aliofkhazraei, M. (2017). Incorporating the principles of shot peening for a better understanding of surface mechanical attrition treatment (SMAT) by simulations and experiments. Materials & Design, 116, 365–373.doi:10.1016/j.matdes.2016.12.045

[33] MEO, M. and VIGNJEVIC, R. (2003). Finite element analysis of residual stress induced by shot peening process. Adv. Eng. Softw., 34, 569–575

[34]. Chen, Z., Sun, Z., & Panicaud, B. (2018). Constitutive modeling of TWIP/TRIP steels and numerical simulation of single impact during Surface Mechanical Attrition Treatment. Mechanics of Materials, 122, 69–75.doi:10.1016/j.mechmat.2018.04.005

[35] Ramin Ghelichi, Giorgio Crispiatico, Mario Guagliano and Sara Bagherifard (2018). An Energetic Approach to Predict the Effect of Shot Peening-Based Surface Treatments. Metals 2018, 8, 190; DOI:10.3390/met8030190

[36] Kirk, D. Prediction and Control of Indent Diameter. In The Shot Peener; 2004; pp. 18–21

[37] Iida, K. Dent and affected layer produced by shot peening. In The Shot Peener; 2000; pp. 4–7

[38]. Sanjurjo, P., Rodríguez, C., Peñuelas, I., García, T. E., & Belzunce, F. J. (2014). Influence of the target material constitutive model on the numerical simulation of a shot peening process. Surface and Coatings Technology, 258, 822–831.doi:10.1016/j.surfcoat.2014.07.075

[39]http://asm.matweb.com/search/SpecificMaterial.asp?bassnum=mq304a

[40] S.Y. Kong & A.M. Remennikov. The Effect of medium strain rates on the mechanical properties of high performance steels

[41]MIAO, H. Y., LAROSE, S., PERRON, C. and L´EVESQUE, M. (2009). On the potential applications of a 3D random finite element model for the simulation of shot peening. Adv. Eng. Softw., 40, 1023–1038

[42] MEGUID, S. A., SHAGAL, G. and STRANART, J. C. (2002). 3D FE analysis of peening of strain-rate sensitive materials using multiple impingement model. Int. J. Impact Eng., 27, 119–134

**[**43] Tao, N. R., Wang, Z. B., Tong, W. P., Sui, M. L., Lu, J., & Lu, K. (2002). *An investigation of surface nanocrystallization mechanism in Fe induced by surface mechanical attrition treatment. Acta Materialia, 50(18), 4603–4616.*doi:10.1016/s1359-6454(02)00310-5

[44] Zhang, X., Lu, J., & Shi, S. (2011). *A Computational Study of Plastic Deformation in AISI 304 Induced by Surface Mechanical Attrition Treatment. Mechanics of Advanced Materials and Structures, 18(8), 572–577.*doi:10.1080/15376494.2011.621828

[45] Wang, J., Han, J., Li, W., Yang, Z., Li, Z., & Zhao, Y. (2016). *Analytical modelling of shot-peening residual stress on welding carbon steel surface layer. Journal of Wuhan University of Technology-Mater. Sci. Ed., 31(6), 1352–1362.* doi:10.1007/s11595-016-1538-x